Random Vortex Method for 2D Incompressible Flows

Shuheng Zhang
St. Peter's College
University of Oxford

A thesis submitted for the degree of
Master of Science in Mathematical Sciences

Trinity 2025

Acknowledgements

I would like to express my deepest gratitude to Professor Zhongmin Qian for his invaluable supervision and continuous support throughout this project. I am also grateful to Vladislav Cherepanov for his insightful suggestions on the presentation of this work. I thank the Mathematical Institute of the University of Oxford and St. Peter's College for providing an inspiring academic environment. Finally, I am profoundly thankful to my parents for their unwavering encouragement, patience, and love.

Abstract

Incompressible viscous fluid flows, central to many physical and engineering applications, are governed by the Navier–Stokes equations. Their vorticity formulation provides both analytical clarity and computational difficulty, especially near boundaries. This dissertation develops a unified stochastic framework based on the random vortex method for simulating two-dimensional incompressible flows across four geometries: the full plane, the upper half-plane, wedge-shaped corner domains, and belt domains bounded by parallel walls. By reformulating vorticity dynamics through probabilistic representations and Monte Carlo methods, we recover classical results in unbounded settings and introduce new techniques for wall-bounded flows. These include reflection-based Biot–Savart kernels, mollified boundary layer corrections, and boundary vorticity dynamics that retain high-order derivative terms. The resulting methods broaden the applicability of vortex-based solvers and offer improved accuracy in capturing near-wall behavior in viscous flows.

Contents

1 Introduction **1**

2 Vortex Formulation and Some Basic Facts **3**

2.1 Derivation of Vorticity Formulation 3

2.2 Key Ideas of the Random Vortex Method 4

3 Flows in Unbounded Domain **6**

3.1 Biot–Savart Law 6

3.2 Stochastic Representation and Closed System of Vortices 8

3.3 Mollification and Numerical Scheme 11

3.4 Simulation 13

4 Flows in Upper Half-Plane **14**

4.1 Biot–Savart in D 15

4.2 Boundary Perturbation 16

4.3 Stochastic Representation of W^ε 17

4.4 Stochastic Representation of the Velocity Field via Mirrored Process . 19

4.5 Approximate Representation of u 21

4.6 Numerical Scheme for u 22

4.7 Boundary Vorticity Dynamics 23

4.8 Simulation 25

5 Flows in Corner Domain **28**

5.1 Biot–Savart Law in the Corner Domain 28

5.2 Boundary Layer Correction 29

5.3 Approximation Formula for u 31

5.4 Numerical Scheme for u 32

5.5 Simulation 33

6 Flows in Belt Domain **35**
6.1 Biot–Savart 35
6.2 Extended velocity field 36
6.3 Velocity evaluation via perturbation decomposition 37
6.4 Boundary Vorticity Evolution Equation 39
6.5 Simulation 40

7 Discussion **42**

8 Conclusion **44**

Bibliography **45**

List of Figures

3.1 Streamline evolution of two vortices with opposite or same circulation in the unbounded domain $\mathbb{R}^2$ with domain $[-1,1]^2$, viscosity $\nu = 0.001$, final time $T = 10.0$. 13

4.1 Streamline evolution in the upper half-plane domain $D = \{x_2 > 0\}$, with viscosity $\nu = 0.1$, time step $\Delta t = 0.1$, and final time $T = 20$. . . 27

5.1 Streamline evolution in the corner domain $Q = \{x_1 > 0,\ x_2 > 0\}$, with viscosity $\nu = 0.1$, time step $\Delta t = 0.1$, and final time $T = 20$. 34

6.1 Streamline evolution in the belt domain $D = \mathbb{R} \times [0,6]$, with viscosity $\nu = 0.05$, time step $\Delta t = 0.1$, and final time $T = 20$. 41

Chapter 1

Introduction

Incompressible viscous fluid flows are fundamental in both theoretical and applied contexts, ranging from atmospheric and oceanic modeling to engineering and biomedical applications. In two spatial dimensions, these flows are governed by the Navier–Stokes equations, whose vorticity formulation provides a powerful reduction: the scalar vorticity $\omega = \nabla \times u$ evolves under the influence of advection, diffusion, and external forcing according to

$$\frac{\partial \omega}{\partial t} + (u \cdot \nabla)\omega - \nu \Delta \omega = G, \tag{1.1}$$

where $\nu > 0$ is the kinematic viscosity and $G = \nabla \times F$ represents the curl of the applied force. The random vortex method builds on this formulation by describing fluid motion via stochastic Lagrangian particles that approximate the transport and diffusion of vorticity—an approach especially amenable to Monte Carlo simulation in complex flow environments.

Historically, particle-based vortex methods were introduced to study inviscid or weakly viscous flows. The point vortex method, tracing back to Helmholtz and Kelvin and later developed computationally in works such as Chorin [3], allowed the representation of vorticity as a sum of Dirac masses transported by the flow. However, this model fails to incorporate viscous effects and becomes increasingly inaccurate in boundary-layer dominated regimes. The emergence of the random vortex method by Chorin and its rigorous convergence established by Goodman [6] and Long [9] marked a turning point: by coupling Lagrangian particle motion with Brownian diffusion, it became possible to stochastically simulate viscous fluid flows in an efficient, probabilistically consistent framework.

Recent advances have extended the random vortex method beyond unbounded domains. Building upon probabilistic tools such as Feynman–Kac representations and McKean–Vlasov stochastic differential equations, Qian and collaborators [13,

12, 1] established rigorous stochastic formulations for incompressible flows in wall-bounded geometries. A particularly notable result is the derivation of a dynamic boundary vorticity equation [1], which reveals that boundary layers evolve under a heat-type equation with doubled viscosity—a striking insight into near-wall behavior. These works highlight the need for boundary-aware Monte Carlo schemes, especially when classical Eulerian methods become computationally prohibitive or ill-suited for stochastic boundary layer phenomena.

This dissertation builds upon this modern shift in perspective. Starting from the classical full-plane case, we develop a unified framework for applying the random vortex method to a variety of two-dimensional geometries, including the upper half-plane, wedge-shaped corner domains, and belt domains bounded by two parallel walls. Our contributions include refined Biot–Savart kernels via geometric reflection, boundary layer corrections using mollified vorticity extensions, and stochastic representations that retain higher-order boundary terms. These developments are motivated by the goal of extending the functional SDE-based approach to more realistic and numerically challenging configurations, with particular attention to boundary vorticity dynamics and their role in closing the system.

The structure of the dissertation is as follows. Chapter 2 introduces the vorticity formulation of the Navier–Stokes equations and reviews the random vortex method. Chapter 3 discusses unbounded flows in $\mathbb{R}^2$, serving as a baseline case. Chapter 4, Chapter 5, and Chapter 6 treat wall-bounded domains of increasing geometric complexity: the half-plane, corner, and belt configurations. The concluding sections summarizes the main findings and outlines directions for future research, including potential extensions to three-dimensional flows and higher-order boundary models.

Chapter 2

Vortex Formulation and Some Basic Facts

This section derives the vorticity formulation of the incompressible Navier–Stokes equations in two dimensions and introduces the core ideas of the random vortex method. We first present the mathematical derivation of the vorticity equation, then outline its probabilistic interpretation, which motivates a particle-based simulation approach.

2.1 Derivation of Vorticity Formulation

Let $u(x,t) = (u_1(x,t), u_2(x,t)) \in \mathbb{R}^2$ denote the velocity field of a two-dimensional viscous incompressible fluid at position $x = (x_1, x_2) \in \mathbb{R}^2$ and time $t \geq 0$. The scalar field $p(x,t)$ represents pressure, $\nu > 0$ is the kinematic viscosity, and $F(x,t) = (F_1(x,t), F_2(x,t))$ denotes a prescribed external body force.

The motion of the fluid is governed by the incompressible Navier–Stokes equations:

$$\frac{\partial u}{\partial t} + (u \cdot \nabla)u = -\nabla p + \nu \Delta u + F, \tag{2.1}$$

subject to the incompressibility condition:

$$\nabla \cdot u = 0, \tag{2.2}$$

which enforces conservation of mass.

To isolate the rotational component of the flow, we define the scalar *vorticity* $\omega(x,t)$ as

$$\omega := \nabla \times u = \frac{\partial u_2}{\partial x_1} - \frac{\partial u_1}{\partial x_2}. \tag{2.3}$$

This quantity characterizes the local angular rotation of fluid elements.

Taking the curl of the momentum equation (2.1), and using the vector identity

$$\nabla \times ((u \cdot \nabla)u) = (u \cdot \nabla)\omega - (\omega \cdot \nabla)u,$$

together with the incompressibility equation (2.2), we obtain the three-dimensional vorticity equation:

$$\frac{\partial \omega}{\partial t} + (u \cdot \nabla)\omega - (\omega \cdot \nabla)u = \nu \Delta \omega + \nabla \times F. \tag{2.4}$$

In the two-dimensional setting, ω becomes a scalar field and the vortex stretching term $(\omega \cdot \nabla)u$ vanishes identically. Therefore, equation (2.4) reduces to

$$\frac{\partial \omega}{\partial t} + (u \cdot \nabla)\omega = \nu \Delta \omega + G, \tag{2.5}$$

where $G := \nabla \times F$ is the scalar curl of the external forcing. This scalar advection–diffusion equation governs the evolution of vorticity in two-dimensional incompressible viscous flows.

The vorticity formulation eliminates the pressure term and yields a single scalar equation for ω, which plays a central role in the development of particle-based methods for simulating viscous fluid flows.

2.2 Key Ideas of the Random Vortex Method

The *random vortex method* offers a probabilistic framework for solving the vorticity equation equation (2.5). The core idea is to interpret the transport–diffusion dynamics of vorticity as the ensemble behavior of randomly moving fluid particles. This connection is formalized through the theory of stochastic differential equations (SDEs) and the Feynman–Kac representation.

Let X_t denote the stochastic trajectory of a vortex particle governed by the SDE:

$$dX_t = u(X_t, t)\, dt + \sqrt{2\nu}\, dB_t, \tag{2.6}$$

where B_t is a standard two-dimensional Brownian motion. This model describes particles that are advected by the flow field u while diffusing due to viscosity. The process X_t is known as the *Taylor diffusion*, a name originating from Taylor's classical analysis of dispersion in shear flows [14].

Under suitable conditions, the solution $\omega(x, t)$ admits the following stochastic representation:

$$\omega(x, t) = \mathbb{E}[\omega_0(X_0) \mid X_t = x] + \int_0^t \mathbb{E}[G(X_s, s) \mid X_t = x]\, ds, \tag{2.7}$$

where ω_0 denotes the initial vorticity and $G := \nabla \times F$ is the curl of the external force. This is known as the *backward representation* of vorticity, derived via adjoint analysis and duality with the Kolmogorov forward equation (see [13, 10]).

This stochastic formulation motivates a Monte Carlo algorithm for approximating vorticity fields: one simulates a large number of particles following equation (2.6), evaluates ω_0 and G along their trajectories, and averages the contributions conditioned on arrival at x at time t. The velocity field u is then reconstructed from ω via the Biot–Savart relation, completing the feedback loop.

Compared to the classical *point vortex method* [4, 10], which approximates vorticity by a sum of Dirac measures

$$\omega(x,t) = \sum_{j=1}^{N} \Gamma_j \delta(x - X_j(t)), \tag{2.8}$$

and evolves them via deterministic ODEs, the random vortex method exhibits several key advantages. The point vortex method is applicable only to inviscid (Euler) flows, lacks any representation of diffusion, and requires careful regularization to avoid singularities. Moreover, it does not naturally accommodate boundary conditions or wall-induced vorticity.

By contrast, the random vortex method inherently models viscosity through Brownian motion, extends naturally to wall-bounded geometries, and enables the inclusion of boundary vorticity. Recent work by Qian and collaborators [13, 1] has established convergence of the empirical particle approximation to the true solution, with an error of order $\mathcal{O}(N^{-1/2})$ under mild assumptions.

The remainder of this dissertation builds on this framework. We begin with the unbounded full-plane case, where the method is most transparent, and then proceed to geometries with increasing complexity: domains with one wall, corner configurations, and belt-shaped regions. Each setting presents distinct analytical and numerical challenges that are addressed in turn.

Chapter 3

Flows in Unbounded Domain

We begin our study of the random vortex method by considering the simplest setting: incompressible viscous flow in the whole plane $\mathbb{R}^2$, where the vorticity dynamics are unaffected by boundaries.

3.1 Biot–Savart Law

To reconstruct the velocity field u from a given vorticity distribution ω in $\mathbb{R}^2$, we appeal to the Biot–Savart law. This relation arises from solving a Poisson equation involving the vorticity and plays a central role in vorticity-based formulations of incompressible flows.

We begin with a key identity that connects u and ω in two dimensions.

Lemma 3.1 (Poisson equation for u and ω)**.** *Let $u = (u_1, u_2)$ be a divergence-free velocity field in $\mathbb{R}^2$, and let $\omega := \nabla \times u = \partial_{x_1} u_2 - \partial_{x_2} u_1$ denote the scalar vorticity. Then,*

$$\Delta u = \nabla \times \omega, \tag{3.1}$$

where $\nabla \times \omega := (-\partial_{x_2}\omega, \partial_{x_1}\omega)$.

Proof. Let $u = (u_1, u_2)$. First, compute the vorticity:

$$w := \nabla \times u = \frac{\partial u_2}{\partial x_1} - \frac{\partial u_1}{\partial x_2}.$$

Now, embed w as the third component in $\mathbb{R}^3$, and take the curl of $(0, 0, w)$:

$$\nabla \times (0, 0, w) = \left(\frac{\partial w}{\partial x_2}, -\frac{\partial w}{\partial x_1}, 0 \right).$$

Using the incompressibility condition $\nabla \cdot u = 0$, we compute:

$$\begin{aligned}\frac{\partial w}{\partial x_2} &= \frac{\partial}{\partial x_2}\left(\frac{\partial u_2}{\partial x_1} - \frac{\partial u_1}{\partial x_2}\right) = \frac{\partial^2 u_2}{\partial x_1 \partial x_2} - \frac{\partial^2 u_1}{\partial x_2^2} \\ &= \frac{\partial}{\partial x_1}\left(-\frac{\partial u_1}{\partial x_1}\right) - \frac{\partial^2 u_1}{\partial x_2^2} = -\frac{\partial^2 u_1}{\partial x_1^2} - \frac{\partial^2 u_1}{\partial x_2^2} = -\Delta u_1.\end{aligned}$$

Similarly,

$$\begin{aligned}\frac{\partial w}{\partial x_1} &= \frac{\partial}{\partial x_1}\left(\frac{\partial u_2}{\partial x_1} - \frac{\partial u_1}{\partial x_2}\right) = \frac{\partial^2 u_2}{\partial x_1^2} - \frac{\partial^2 u_1}{\partial x_1 \partial x_2} \\ &= \frac{\partial^2 u_2}{\partial x_1^2} - \frac{\partial}{\partial x_2}\left(-\frac{\partial u_2}{\partial x_2}\right) = \frac{\partial^2 u_2}{\partial x_1^2} + \frac{\partial^2 u_2}{\partial x_2^2} = \Delta u_2.\end{aligned}$$

Hence,

$$\Delta u = (\Delta u_1, \Delta u_2) = \left(-\frac{\partial w}{\partial x_2}, \frac{\partial w}{\partial x_1}\right) = \nabla \times w.$$

□

This identity implies that u can be recovered from ω by solving a Poisson equation with source term $\nabla \times \omega$. The corresponding fundamental solution in $\mathbb{R}^2$ is given by the logarithmic potential:

Lemma 3.2 (Fundamental solution of Poisson's equation in $\mathbb{R}^2$)**.** *Let $G(x) := -\frac{1}{2\pi}\log|x|$. Then, for any compactly supported smooth function f,*

$$\phi(x) := \int_{\mathbb{R}^2} G(x-y) f(y)\, dy$$

solves $-\Delta\phi = f$ in the distributional sense.

We omit the proof and refer to standard PDE text such as Evans [5].

Theorem 3.3 (Biot–Savart Law in $\mathbb{R}^2$)**.** *Let $\omega \in C_c^\infty(\mathbb{R}^2)$ be a compactly supported smooth vorticity field. Then the velocity field u is given by*

$$u(x,t) = \int_{\mathbb{R}^2} K(x-y)\, \omega(y,t)\, dy, \tag{3.2}$$

where the Biot–Savart kernel K is

$$K(x) := \left(\frac{\partial G}{\partial x_2}, -\frac{\partial G}{\partial x_1}\right) = \frac{1}{2\pi}\left(-\frac{x_2}{|x|^2}, \frac{x_1}{|x|^2}\right). \tag{3.3}$$

Proof. From Lemmas Theorem 3.1 and Theorem 3.2, we write

$$u(x) = \int_{\mathbb{R}^2} G(x-y)(-\nabla \times \omega)(y)\, dy.$$

Using integration by parts, justified by the compact support of ω and the decay of G, we compute:

$$u_1(x) = \int_{\mathbb{R}^2} G(x-y) \left(-\frac{\partial \omega}{\partial y_2}\right) dy = \int_{\mathbb{R}^2} \frac{\partial G}{\partial y_2}(x-y)\, \omega(y)\, dy,$$
$$u_2(x) = \int_{\mathbb{R}^2} G(x-y) \left(\frac{\partial \omega}{\partial y_1}\right) dy = -\int_{\mathbb{R}^2} \frac{\partial G}{\partial y_1}(x-y)\, \omega(y)\, dy.$$

Using $\partial G/\partial y_i = -\partial G/\partial x_i$, we obtain the result:

$$u(x) = \int_{\mathbb{R}^2} K(x-y)\, \omega(y)\, dy.$$

□

The Biot–Savart law expresses the velocity as a convolution of the vorticity with a singular kernel. This nonlocal relation is central to vortex methods and will be used throughout this work, both in unbounded and bounded domain formulations.

From this point forward, we adopt the notation $K(x,y) := K(x-y)$ to denote the Biot–Savart kernel evaluated at points x and y in $\mathbb{R}^2$, where

$$K(x) = \frac{1}{2\pi}\left(-\frac{x_2}{|x|^2}, \frac{x_1}{|x|^2}\right)$$

is the standard singular kernel. This two-point notation $K(x,y)$ is convenient for generalizations to bounded domains and will be used consistently throughout the rest of this dissertation.

3.2 Stochastic Representation and Closed System of Vortices

We now describe how the two-dimensional vorticity equation in an unbounded domain admits a natural probabilistic interpretation and formulate the resulting closed-loop system underlying the random vortex method. For clarity, we consider the case without external forcing.

Assuming $G = 0$, the vorticity field $w(x,t)$ satisfies the linear parabolic equation

$$\frac{\partial w}{\partial t} + (u \cdot \nabla) w = \nu \Delta w, \tag{3.4}$$

where the velocity field $u(x,t)$ is divergence-free and sufficiently smooth. Define the linear operator

$$L := \nu\Delta - (u \cdot \nabla),$$

so that equation (3.4) becomes

$$\left(\frac{\partial}{\partial t} - L\right) w = 0.$$

The solution to this equation can be expressed in terms of a fundamental solution.

Lemma 3.4 (Fundamental solution of the linearized vorticity equation)**.** *Let w_0 be a given initial vorticity distribution. A function $\Gamma(x,t;\xi,0)$ is called the* fundamental solution *(or Green's function) of the operator L if it satisfies*

$$\left(\frac{\partial}{\partial t} - L\right)\Gamma(x,t;\xi,0) = 0, \qquad \lim_{t\to 0+}\Gamma(x,t;\xi,0) = \delta(x-\xi), \tag{3.5}$$

where δ is the Dirac delta function. Then the solution to equation (3.4) *with initial data w_0 is given by*

$$w(x,t) = \int_{\mathbb{R}^2} \Gamma(x,t;\xi,0)\, w_0(\xi)\, d\xi. \tag{3.6}$$

We omit the proof, as this result can be found in standard PDE text (e.g., Evans [5]).

Although an explicit formula for Γ is rarely available, a powerful result from stochastic analysis allows us to interpret it probabilistically as the transition density of a diffusion process. Consider the stochastic differential equation (SDE)

$$dX_t = u(X_t,t)\, dt + \sqrt{2\nu}\, dB_t, \qquad X_0 = \xi, \tag{3.7}$$

where B_t is a standard two-dimensional Brownian motion. The following lemma connects the transition density of X_t with the PDE operator L.

Lemma 3.5 (Kolmogorov backward equation)**.** *Let X_t solve the SDE equation* (3.7)*, and let $p(0,\xi;t,x)$ denote its transition probability density, i.e.,*

$$p(0,\xi;t,x)\, dx = \mathbb{P}(X_t \in dx \mid X_0 = \xi).$$

Then p satisfies the Kolmogorov backward equation:

$$\left(\frac{\partial}{\partial t} - L^\star\right) p(0,\xi;t,x) = 0, \tag{3.8}$$

where the backward operator is given by

$$L^\star := \nu\Delta_x - u(x,t)\cdot\nabla_x.$$

The proof is omitted here and can be found in standard SDE texts, such as Øksendal [11, Chapter 7]. This result implies that the fundamental solution $\Gamma(x,t;\xi,0)$ coincides with the transition density of X_t. Hence, the solution to equation (3.4) can be expressed as

$$w(x,t) = \mathbb{E}[w_0(X_0) \mid X_t = x], \tag{3.9}$$

a form known as the *backward Kolmogorov representation* or *Feynman–Kac formula*. This identity underpins the random vortex method.

We now couple the probabilistic representation of vorticity with the Biot–Savart law. Recall that the velocity field is recovered from the vorticity via

$$\begin{aligned} u(x,t) &= \int_{\mathbb{R}^2} K(x,y)\, w(y,t)\, dy \\ &= \int_{\mathbb{R}^2} K(x,y)\, \mathbb{E}[w_0(X_0) \mid X_t = y]\, dy \\ &= \mathbb{E}\left[\int_{\mathbb{R}^2} K(x, X_t^\xi)\, w_0(\xi)\, d\xi\right] \\ &= \int_{\mathbb{R}^2} \mathbb{E}[K(x, X_t^z)]\, w_0(z)\, dz, \end{aligned} \tag{3.10}$$

where K is the Biot–Savart kernel, and X_t^ξ denotes the solution to the SDE equation (3.7) starting from initial position ξ. In the third line, we apply Fubini's theorem to exchange the expectation and integration; in the final line, we relabel ξ as z for notational consistency.

This identity defines a closed-loop stochastic system in which the particle trajectories and the velocity field are coupled:

$$\begin{cases} dX_t = u(X_t,t)\, dt + \sqrt{2\nu}\, dB_t, \\ X_0 = z \in \mathbb{R}^2, \\ u(x,t) = \displaystyle\int_{\mathbb{R}^2} \mathbb{E}[K(x, X_t^z)]\, w_0(z)\, dz. \end{cases} \tag{3.11}$$

This nonlinear system forms the foundation of the random vortex method in unbounded domains: particles evolve according to a velocity field they themselves help generate, thereby closing the stochastic formulation of the incompressible vorticity equation.

3.3 Mollification and Numerical Scheme

The Biot–Savart law expresses the velocity field $u(x,t)$ as a convolution of the vorticity field $w(y,t)$ with the singular kernel $K(x,y)$:

$$u(x,t) = \int_{\mathbb{R}^2} K(x,y)\, w(y,t)\, dy. \tag{3.12}$$

While this expression is mathematically well-defined for smooth w, it poses numerical challenges due to the singularity of $K(x,y) \sim \frac{1}{|x-y|}$ as $x \to y$. Near-singular interactions between particles can lead to instability and inaccurate velocity evaluations in simulations.

To address this, we introduce a mollification procedure that smooths the kernel K near the singularity while preserving its behavior at large distances.

Definition 3.6 (Mollifier)**.** *A* mollifier *is a smooth, non-negative, compactly supported, radially symmetric function $\psi \in C_0^\infty(\mathbb{R}^2)$ satisfying the normalization condition:*

$$\int_{\mathbb{R}^2} \psi(x)\, dx = 1.$$

Given a smoothing parameter $\delta > 0$, we define the scaled mollifier:

$$\psi_\delta(x) := \frac{1}{\delta^2}\psi\left(\frac{x}{\delta}\right).$$

Lemma 3.7 (Mollified Biot–Savart Kernel)**.** *Let $K(x)$ be the Biot–Savart kernel in $\mathbb{R}^2$,*

$$K(x) = \frac{1}{2\pi}\left(-\frac{x_2}{|x|^2}, \frac{x_1}{|x|^2}\right),$$

which is singular at the origin. Let ψ_δ be a scaled mollifier as in Definition 3.6. Then the mollified Biot–Savart kernel is defined via convolution:

$$K_\delta(x) := (K * \psi_\delta)(x) = \int_{\mathbb{R}^2} K(x,y)\, \psi_\delta(y)\, dy.$$

This mollified kernel $K_\delta(x)$ is smooth and bounded for all $x \in \mathbb{R}^2$.

A convenient and computationally efficient representation of the mollified kernel takes the form

$$\begin{aligned} K_\delta(x) &= K(x) \cdot f\left(\frac{|x|}{\delta}\right), \\ f(r) &= 2\pi \int_0^r s\psi(s)\, ds, \end{aligned} \tag{3.13}$$

where the cutoff function $f(r)$ regularizes the kernel near $r = 0$ while preserving the asymptotics of K as $r \to \infty$. This expression is discussed in [10, p. 209].

In our numerical implementation, we adopt the specific form

$$f(r) = 1 - \exp\left(-\left(\frac{r}{\delta}\right)^2\right),$$

which satisfies $f(0) = 0$, $f(r) \to 1$ as $r \to \infty$, and transitions smoothly between these extremes. This choice ensures the mollified kernel $K_\delta(x, y) := K_\delta(x - y)$ remains stable and accurate even when $x \approx y$. For the remainder of this work, we assume all kernels $K(x, y)$ are mollified by default unless otherwise noted.

After mollification, we discretize the vorticity field over a uniform grid with spacing h, assigning a vortex particle to each grid point. The velocity is then approximated via a weighted Riemann sum, and the particles evolve according to the Euler–Maruyama scheme for the SDE (3.7). The following algorithm summarizes the full numerical scheme.

Algorithm 1 Random Vortex Method: Velocity Computation and Particle Advection

1: **Initialization:** Discretize the initial vorticity w_0 on a uniform grid $\xi \in h\mathbb{Z}^2$, and assign vortex particles with initial position $X_0^\xi = \xi$ and vorticity strength $w_0^\xi = w_0(\xi)$.
2: **for** each time step $k = 0, 1, \ldots, N - 1$ **do**
3: **Compute velocity field:**

$$u(x, t_k) \approx \sum_\xi K_\delta(x, X_k^\xi)\, w_k^\xi\, h^2,$$

where X_k^ξ is the position of the particle labeled ξ at time t_k, and w_k^ξ is its vorticity.
4: **for** each particle ξ **do**
5: Evaluate $u(X_k^\xi, t_k)$ by summing mollified Biot–Savart contributions.
6: **Update particle position via Euler–Maruyama:**

$$X_{k+1}^\xi = X_k^\xi + u(X_k^\xi, t_k)\Delta t + \sqrt{2\nu\Delta t} \cdot \eta_k^\xi,$$

where $\eta_k^\xi \sim \mathcal{N}(0, I_2)$ models Brownian motion.
7: **end for**
8: **end for**

This algorithm approximates the vorticity transport–diffusion equation by tracking particles that move under both advection and diffusion. The mollification ensures stable velocity evaluation even in regions of high particle concentration. This basic algorithm underpins all future simulations in this dissertation. In later sections, we will

modify the kernel $K_\delta(x, y)$ and velocity function to account for boundary conditions, or adapt the SDE when geometry constraints (e.g., belt domain) require reflected or transformed dynamics.

3.4 Simulation

We simulate the evolution of two point vortices in the unbounded domain $\mathbb{R}^2$. The vortices are initialized at $(-0.5, 0)$ and $(0.5, 0)$ on a 21×21 grid over $[-1, 1]^2$, with only these two grid points carrying nonzero vorticity. We consider two circulation configurations: equal and opposite signs, and equal and positive signs. The velocity field is computed using a mollified Biot–Savart kernel with smoothing parameter $\delta = 0.1$, and each vortex is represented by $N = 10$ stochastic particles. The viscosity is set to $\nu = 0.001$, and the SDE is integrated using the Euler–Maruyama scheme with time step $\Delta t = 0.1$ up to final time $T = 10.0$.

Figure 3.1 shows the streamline evolution for both cases. Opposite-sign vortices attract and form a dipole that translates steadily across the domain. Same-sign vortices rotate around their common center, maintaining a circular orbit. Despite the presence of diffusion, the coherent structures are preserved. Minor asymmetries appear due to Brownian motion, especially at later times, illustrating the trade-off between physical realism and stochastic variability in the random vortex method.

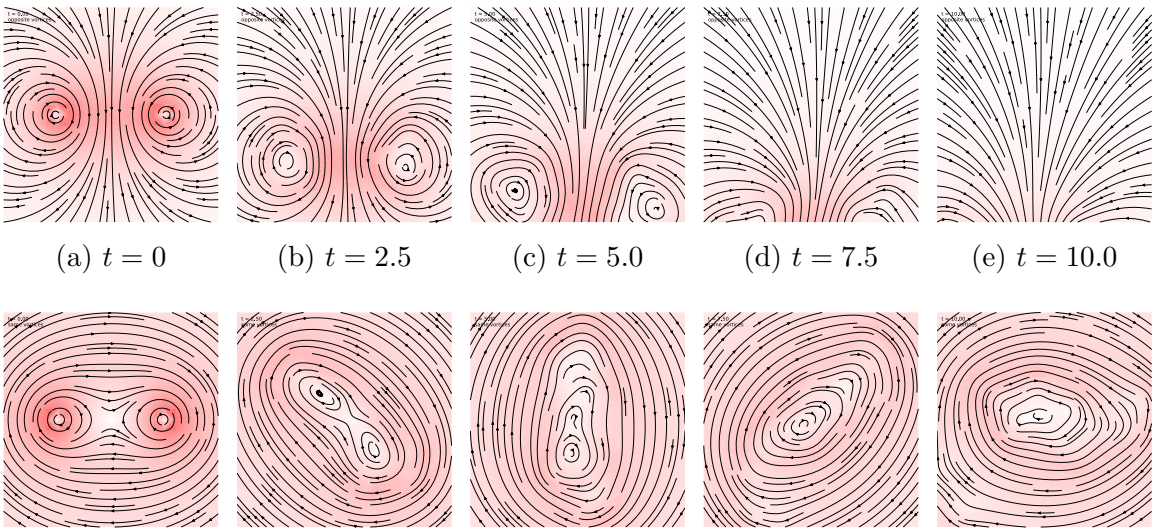

(a) $t = 0$ (b) $t = 2.5$ (c) $t = 5.0$ (d) $t = 7.5$ (e) $t = 10.0$

(f) $t = 0$ (g) $t = 2.5$ (h) $t = 5.0$ (i) $t = 7.5$ (j) $t = 10.0$

Figure 3.1: Streamline evolution of two vortices with opposite or same circulation in the unbounded domain $\mathbb{R}^2$ with domain $[-1, 1]^2$, viscosity $\nu = 0.001$, final time $T = 10.0$.

Chapter 4

Flows in Upper Half-Plane

We now extend the random vortex method to a wall-bounded geometry by considering incompressible viscous flow in the upper half-plane:

$$D := \mathbb{H} = \{(x_1, x_2) \in \mathbb{R}^2 \,:\, x_2 > 0\}.$$

The velocity field $u(x,t)$ is subject to an external force field $F(x,t)$ and must satisfy the classical *no-slip boundary condition* along the wall at $x_2 = 0$:

$$u|_{\partial D} = 0.$$

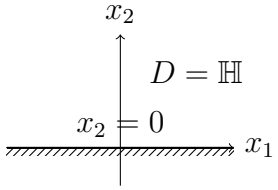

To account for the boundary, we modify the Biot–Savart law using a *reflection principle* to construct a velocity kernel that vanishes along the wall. We then decompose the vorticity into a bulk component and a boundary layer correction, and introduce a cutoff profile to localize the wall-induced vorticity. This yields a perturbed vorticity equation with homogeneous boundary conditions, which we solve using a stochastic representation based on Taylor diffusion. The resulting method retains the mesh-free nature of the vortex formulation while respecting the no-slip condition, and forms the basis for our numerical scheme in wall-bounded domains.

4.1 Biot–Savart in D

We derive the Biot–Savart law for the upper half-plane $D = \mathbb{H} = \{x = (x_1, x_2) \in \mathbb{R}^2 : x_2 > 0\}$, where the velocity field must vanish on the boundary $\partial D = \{x_2 = 0\}$. To enforce the Dirichlet condition, we construct a Green's function via reflection across the wall.

Lemma 4.1 (Green's function in the upper half-plane)**.** *Let $G(x) = -\frac{1}{2\pi} \log |x|$ be the fundamental solution to the Laplace equation in $\mathbb{R}^2$, and define the reflection of $x = (x_1, x_2)$ as $\overline{x} = (x_1, -x_2)$. Set*

$$G_D(x) := G(x) - G(\overline{x}) = -\frac{1}{2\pi} \log \left(\frac{|x|}{|\overline{x}|} \right).$$

Then the function

$$u(x) = \int_D G_D(x - y)\, f(y)\, dy$$

solves $\Delta u = f$ in D, with zero Dirichlet boundary condition $u|_{\partial D} = 0$.

Sketch of proof. The Laplacian commutes with reflection, so

$$-\Delta G_D(x) = \delta(x) - \delta(\overline{x}).$$

Therefore, for $x \in D$,

$$\Delta u(x) = \int_D \left[-\delta(x - y) + \delta(x - \overline{y}) \right] f(y)\, dy = f(x),$$

since $\overline{y} \notin D$. On the boundary $x_2 = 0$, $\overline{x} = x$, so $G_D(x - y) = 0$ and $u(x) = 0$. □

Corollary 4.2 (Biot–Savart law in the upper half-plane)**.** *Let $\omega(x, t)$ be a vorticity field in D. Then the corresponding velocity field $u(x, t)$, satisfying $u|_{\partial D} = 0$, is given by*

$$u(x, t) = \int_D K_D(x, y)\, \omega(y, t)\, dy,$$

where the modified Biot–Savart kernel is

$$K_D(x, y) = \frac{1}{2\pi} \left(-\left[\frac{x_2 - y_2}{|x - y|^2} - \frac{x_2 + y_2}{|x - \overline{y}|^2} \right], \ \left[\frac{x_1 - y_1}{|x - y|^2} - \frac{x_1 - y_1}{|x - \overline{y}|^2} \right] \right).$$

Proof. The result follows from the standard Biot–Savart derivation, using the reflected Green's function G_D in place of the fundamental solution. Boundary terms vanish due to the compact support of ω and the decay of G_D at infinity. □

4.2 Boundary Perturbation

To impose the no-slip boundary condition $u|_{\partial D} = 0$ on the flat wall $\partial D = \{x_2 = 0\}$, we modify the vorticity formulation so that the resulting system admits a zero-boundary vorticity field. This enables the use of Dirichlet-type Green's functions and stochastic representations within the upper half-plane $D = \mathbb{H}$.

We isolate the boundary vorticity as

$$\theta(x_1, t) := \omega(x_1, 0, t),$$

and introduce a smooth cutoff function $\phi : [0, \infty) \to [0, 1]$, compactly supported near the wall. Following [**?**, Section 3], define:

$$\phi(r) = \begin{cases} 1, & r \in [0, \frac{1}{3}], \\ \frac{1}{2} + 54(r - \frac{1}{2})^3 - \frac{9}{2}(r - \frac{1}{2}), & r \in [\frac{1}{3}, \frac{2}{3}], \\ 0, & r \geq \frac{2}{3}, \end{cases} \tag{4.1}$$

so that $\phi \in C^2$, with derivatives

$$\phi'(r) = \begin{cases} 162(r - \frac{1}{2})^2 - \frac{9}{2}, & r \in [\frac{1}{3}, \frac{2}{3}], \\ 0, & \text{otherwise}, \end{cases} \qquad \phi''(r) = \begin{cases} 324(r - \frac{1}{2}), & r \in [\frac{1}{3}, \frac{2}{3}], \\ 0, & \text{otherwise}. \end{cases}$$

Define the boundary layer correction as

$$\sigma^\varepsilon(x_1, x_2, t) := \theta(x_1, t)\, \phi\left(\frac{x_2}{\varepsilon}\right),$$

and subtract it from the total vorticity:

$$W^\varepsilon(x_1, x_2, t) := \omega(x_1, x_2, t) - \sigma^\varepsilon(x_1, x_2, t),$$

which satisfies $W^\varepsilon(x_1, 0, t) = 0$ for all $x_1 \in \mathbb{R}$.

Substituting into the vorticity equation yields:

$$\left(\frac{\partial}{\partial t} + u \cdot \nabla - \nu\Delta\right) W^\varepsilon = g^\varepsilon(x, t), \qquad W^\varepsilon|_{\partial D} = 0, \tag{4.2}$$

where g^ε collects the residual terms from differentiating σ^ε:

$$\begin{aligned} g^\varepsilon(x, t) = G(x, t) &+ \frac{\nu}{\varepsilon^2}\phi''\left(\frac{x_2}{\varepsilon}\right)\, \theta(x_1, t) - \frac{1}{\varepsilon}\phi'\left(\frac{x_2}{\varepsilon}\right)\, u_2(x, t)\, \theta(x_1, t) \\ &+ \phi\left(\frac{x_2}{\varepsilon}\right)\left[\nu\frac{\partial^2\theta}{\partial x_1^2}(x_1, t) - \frac{\partial\theta}{\partial t}(x_1, t) - u_1(x, t)\,\frac{\partial\theta}{\partial x_1}(x_1, t)\right], \end{aligned} \tag{4.3}$$

where $G := \nabla \times F$ is the vorticity of the external force.

This reformulation transforms the original equation into a homogeneous boundary problem, suitable for Green's function and stochastic methods. The parameter $\varepsilon \ll 1$ sets the thickness of the boundary layer, and the dominant contribution near the wall arises from the singular term $\frac{\nu}{\varepsilon^2}\phi''\theta$, as noted in [**?**]. In practice, the term involving $\phi' \cdot u_2$ is negligible because ϕ' is supported only in a narrow region near the wall and u_2 vanishes at the boundary and remains small nearby. Similarly, the bracketed term is multiplied by the compactly supported $\phi(x_2/\varepsilon)$, making its contribution asymptotically small as $\varepsilon \to 0$. Thus, the source term g^ε may be approximated by its leading-order terms:

$$g^\varepsilon(x,t) \approx G(x,t) + \frac{\nu}{\varepsilon^2}\phi''\left(\frac{x_2}{\varepsilon}\right)\theta(x_1,t).$$

4.3 Stochastic Representation of W^ε

We now derive a stochastic representation for the solution W^ε of the boundary value problem equation (4.2), posed in a bounded domain $D \subset \mathbb{R}^d$ with Lipschitz boundary. This representation expresses $W^\varepsilon(y,t)$ as a conditional expectation over Taylor diffusion paths and forms the probabilistic foundation for our numerical method.

Theorem 4.3 (Stochastic Representation of W^ε)**.** *Let $W^\varepsilon(y,t)$ be a smooth solution to equation* (4.2) *with initial data $W^\varepsilon(\cdot,0)$. Let X_t^ξ denote the Taylor diffusion process defined by the Itô SDE*

$$dX_t^\xi = u(X_t^\xi,t)\,dt + \sqrt{2\nu}\,dB_t, \quad X_0^\xi = \xi,$$

with transition density $p(0,\xi;t,y)$. Then for any $t>0$ and $y \in D$, we have:

$$\begin{aligned} W^\varepsilon(y,t) = &\int_D \mathbb{E}\left[\mathbb{1}_{\{\zeta(X^\xi)>t\}}\, W^\varepsilon(\xi,0) \,\middle|\, X_t^\xi = y\right] p(0,\xi;t,y)\,d\xi \\ &+ \int_0^t \int_D \mathbb{E}\left[\mathbb{1}_{\{s>\gamma_t(X^\xi)\}}\, g^\varepsilon(X_s^\xi,s) \,\middle|\, X_t^\xi = y\right] p(0,\xi;t,y)\,d\xi\,ds. \end{aligned} \tag{4.4}$$

Here, for any continuous path $\psi : [0,t] \to \overline{D}$, define the first exit time and last boundary hitting time by

$$\zeta(\psi) := \inf\{s \geq 0 : \psi(s) \notin D\}, \qquad \gamma_t(\psi) := \sup\{s \in (0,t) : \psi(s) \in \partial D\}.$$

Proof. For simplicity, we drop the superscript ε and write $W = W^\varepsilon$, $g = g^\varepsilon$ throughout the proof.

Fix $t > 0$ and $y \in D$, and define the time-reversed process $\tilde{X}_s^y$ via

$$d\tilde{X}_s^y = -u(\tilde{X}_s^y, t-s)\,ds + \sqrt{2\nu}\,dB_s, \quad \tilde{X}_0^y = y.$$

Let $T_y := \inf\{s \geq 0 : \tilde{X}_s^y \notin D\}$ be the first exit time of $\tilde{X}^y$ from D, and define the auxiliary process

$$Y_s := \mathbb{1}_{\{s<T_y\}}\, W(\tilde{X}_s^y, t-s).$$

Applying Itô's formula to $W(\tilde{X}_s^y, t-s)$, and noting from equation (4.2) that

$$\partial_t W = -u \cdot \nabla W + \nu \Delta W - g,$$

we compute

$$\begin{aligned} dW(\tilde{X}_s^y, t-s) &= \nabla W(\tilde{X}_s^y, t-s) \cdot d\tilde{X}_s^y + \partial_s W(\tilde{X}_s^y, t-s)\,ds + \nu \Delta W(\tilde{X}_s^y, t-s)\,ds \\ &= \nabla W(\tilde{X}_s^y, t-s) \cdot \big[-u(\tilde{X}_s^y, t-s)\,ds + \sqrt{2\nu}\,dB_s \big] \\ &\quad - \partial_t W(\tilde{X}_s^y, t-s)\,ds + \nu \Delta W(\tilde{X}_s^y, t-s)\,ds \\ &= \sqrt{2\nu}\,\nabla W(\tilde{X}_s^y, t-s) \cdot dB_s - g(\tilde{X}_s^y, t-s)\,ds. \end{aligned}$$

Integrating from 0 to $s < T_y$, we obtain

$$W(\tilde{X}_s^y, t-s) = W(y,t) + \sqrt{2\nu} \int_0^s \nabla W(\tilde{X}_r^y, t-r) \cdot dB_r - \int_0^s g(\tilde{X}_r^y, t-r)\,dr.$$

Taking expectations and noting that the stochastic integral vanishes, we get

$$W(y,t) = \mathbb{E}\left[W(\tilde{X}_t^y, 0)\, \mathbb{1}_{\{t<T_y\}} \right] + \int_0^t \mathbb{E}\left[\mathbb{1}_{\{r<T_y\}}\, g(\tilde{X}_r^y, t-r) \right] dr.$$

Conditioning on the event $\tilde{X}_t^y = \xi$, we rewrite the two terms above as

$$\mathbb{E}\left[W(\tilde{X}_t^y, 0)\, \mathbb{1}_{\{t<T_y\}} \right] = \int_D \mathbb{E}\left[W(\xi, 0)\, \mathbb{1}_{\{t<T_y\}} \mid \tilde{X}_t^y = \xi \right] p^{-u}(0, y; t, \xi)\,d\xi,$$

and

$$\int_0^t \mathbb{E}\left[\mathbb{1}_{\{r<T_y\}}\, g(\tilde{X}_r^y, t-r) \right] dr = \int_0^t \int_D \mathbb{E}\left[\mathbb{1}_{\{r<T_y\}}\, g(\tilde{X}_r^y, t-r) \mid \tilde{X}_t^y = \xi \right] p^{-u}(0, y; t, \xi)\,d\xi\,dr.$$

Since u is divergence-free, time-reversal duality implies

$$p^{-u}(0, y; t, \xi) = p(0, \xi; t, y).$$

Moreover, by standard reversal arguments,

$$\mathbb{E}\left[W(\xi,0)\,\mathbb{1}_{\{t<T_y\}} \mid \tilde{X}_t^y = \xi\right] = \mathbb{E}\left[\mathbb{1}_{\{t<\zeta(X^\xi)\}}\, W(\xi,0) \mid X_t^\xi = y\right],$$

$$\mathbb{E}\left[\mathbb{1}_{\{r<T_y\}}\, g(\tilde{X}_r^y, t-r) \mid \tilde{X}_t^y = \xi\right] = \mathbb{E}\left[\mathbb{1}_{\{r>\gamma_t(X^\xi)\}}\, g(X_r^\xi, r) \mid X_t^\xi = y\right].$$

To verify this, let $\psi : [0,t] \to \overline{D}$ be continuous, with $\psi(0) = \xi$, $\psi(t) = y$, and define the time-reversed path $\psi \circ \tau_t(s) = \psi(t-s)$. Then:

$$\{t < \zeta(\psi \circ \tau_t)\} = \{\psi(r) \in D,\ \forall r \in (0,t)\} = \{t < \zeta(\psi)\},$$
$$\{t - r < \zeta(\psi \circ \tau_t)\} = \{\psi(q) \in D,\ \forall q \in (r,t)\} = \{r > \gamma_t(\psi)\}.$$

Combining all terms yields the desired representation:

$$W(y,t) = \int_D \mathbb{E}\left[\mathbb{1}_{\{t<\zeta(X^\xi)\}}\, W(\xi,0) \mid X_t^\xi = y\right]\, p(0,\xi;t,y)\, d\xi + \int_0^t \int_D \mathbb{E}\left[\mathbb{1}_{\{r>\gamma_t(X^\xi)\}}\, g(X_r^\xi, r) \mid X_t^\xi = y\right]\, p(0,\xi;t,y)\, d\xi\, dr.$$

□

Remark. This representation decomposes $W^\varepsilon(y,t)$ into two contributions: one from the initial data and one from the source term g^ε, both conditioned on events related to the behavior of the stochastic trajectory. The result is a special case of Theorem 2.1 in [8] and is central to our Monte Carlo algorithm.

4.4 Stochastic Representation of the Velocity Field via Mirrored Process

We now derive a probabilistic representation of the velocity field $u(x,t)$ in the upper half-plane. This result combines the Biot–Savart law with the stochastic representation of the corrected vorticity W^ε, and leverages the symmetry of the domain through a mirrored diffusion identity.

Lemma 4.4 (Mirrored Process Identity)**.** *Let X_t^ξ be a Taylor diffusion process starting from $\xi \in \overline{D}$, where $D = \{x \in \mathbb{R}^2 : x_2 > 0\}$, and let $\overline{\xi} := (x_1, -x_2)$ be the reflection of ξ across the boundary. Define the exit time*

$$\zeta(X^\xi) := \inf\{s \geq 0 : X_s^\xi \notin D\}.$$

Then for any bounded measurable function $f : \mathbb{R}^2 \to \mathbb{R}$,

$$\mathbb{E}\left[\mathbb{1}_{\{\zeta(X^\xi)>t\}} f(X_t^\xi)\right] = \mathbb{E}\left[\mathbb{1}_D(X_t^\xi)\, f(X_t^\xi)\right] - \mathbb{E}\left[\mathbb{1}_D(X_t^{\overline{\xi}})\, f(X_t^{\overline{\xi}})\right]. \tag{4.5}$$

Proof. Let $p^D(0,\xi;t,y)$ denote the sub-probability density of X_t^ξ killed upon exiting D, given by:

$$p^D(0,\xi;t,y) = p(0,\xi;t,y) - p(0,\xi;t,\overline{y}).$$

In the upper half-plane, the transition density satisfies the symmetry:

$$p(0,\xi;t,y) = p(0,\overline{\xi};t,\overline{y}),$$

so

$$p^D(0,\xi;t,y) = p(0,\xi;t,y) - p(0,\overline{\xi};t,y).$$

Hence, for any bounded measurable function f,

$$\begin{aligned}\mathbb{E}\left[\mathbb{1}_{\{\zeta(X^\xi)>t\}} f(X_t^\xi)\right] &= \int_D f(y)\, p^D(0,\xi;t,y)\, dy \\ &= \int_D f(y)\, p(0,\xi;t,y)\, dy - \int_D f(y)\, p(0,\overline{\xi};t,y)\, dy \\ &= \mathbb{E}\left[\mathbb{1}_D(X_t^\xi)\, f(X_t^\xi)\right] - \mathbb{E}\left[\mathbb{1}_D(X_t^{\overline{\xi}})\, f(X_t^{\overline{\xi}})\right].\end{aligned}$$

□

Proposition 4.5 (Stochastic Representation of the Velocity Field)**.** *Let $\omega = \sigma^\varepsilon + W^\varepsilon$, and let $K_D(x,y)$ denote the Biot–Savart kernel in the upper half-plane. Then the velocity field $u(x,t)$ satisfies:*

$$\begin{aligned}u(x,t) = &\int_D K_D(x,y)\, \sigma^\varepsilon(y,t)\, dy \\ &+ \int_D \mathbb{E}\left[\mathbb{1}_D(X_t^\xi)\, K_D(x,X_t^\xi) - \mathbb{1}_D(X_t^{\overline{\xi}})\, K_D(x,X_t^{\overline{\xi}})\right] W^\varepsilon(\xi,0)\, d\xi \qquad (4.6) \\ &+ \int_0^t \int_D \mathbb{E}\left[\mathbb{1}_{\{s>\gamma_t(X^\xi)\}}\, K_D(x,X_t^\xi)\, g^\varepsilon(X_s^\xi,s)\right] d\xi\, ds.\end{aligned}$$

Proof. From the Biot–Savart law and the decomposition $\omega = \sigma^\varepsilon + W^\varepsilon$, we write:

$$u(x,t) = \int_D K_D(x,y)\, \sigma^\varepsilon(y,t)\, dy + \int_D K_D(x,y)\, W^\varepsilon(y,t)\, dy.$$

We now apply the stochastic representation of W^ε from Theorem 4.3. Using

Fubini's theorem:

$$\begin{aligned}
&\int_D K_D(x,y)\, W^\varepsilon(y,t)\, dy \\
&\quad = \int_D K_D(x,y) \left(\int_D \mathbb{E}\left[\mathbb{1}_{\{\zeta(X^\xi)>t\}}\, W^\varepsilon(\xi,0) \mid X_t^\xi = y \right] p(0,\xi;t,y)\, d\xi \right) dy \\
&\qquad + \int_D K_D(x,y) \left(\int_0^t \int_D \mathbb{E}\left[\mathbb{1}_{\{s>\gamma_t(X^\xi)\}}\, g^\varepsilon(X_s^\xi, s) \mid X_t^\xi = y \right] p(0,\xi;t,y)\, d\xi\, ds \right) dy \\
&\quad = \int_D \mathbb{E}\left[\left(\int_D K_D(x,y)\, p(0,\xi;t,y)\, dy \right) \mathbb{1}_{\{\zeta(X^\xi)>t\}} \right] W^\varepsilon(\xi,0)\, d\xi \\
&\qquad + \int_0^t \int_D \mathbb{E}\left[\mathbb{1}_{\{s>\gamma_t(X^\xi)\}}\, K_D(x, X_t^\xi)\, g^\varepsilon(X_s^\xi, s) \right] d\xi\, ds.
\end{aligned}$$

Applying Lemma 4.4 to the function $f(y) = K_D(x,y)$, we simplify:

$$\mathbb{E}\left[\mathbb{1}_{\{\zeta(X^\xi)>t\}}\, K_D(x, X_t^\xi) \right] = \mathbb{E}\left[\mathbb{1}_D(X_t^\xi)\, K_D(x, X_t^\xi) \right] - \mathbb{E}\left[\mathbb{1}_D(X_t^{\bar{\xi}})\, K_D(x, X_t^{\bar{\xi}}) \right].$$

Hence,

$$\begin{aligned}
\int_D K_D(x,y)\, W^\varepsilon(y,t)\, dy = &\int_D \mathbb{E}\left[\mathbb{1}_D(X_t^\xi)\, K_D(x, X_t^\xi) - \mathbb{1}_D(X_t^{\bar{\xi}})\, K_D(x, X_t^{\bar{\xi}}) \right] W^\varepsilon(\xi,0)\, d\xi \\
&+ \int_0^t \int_D \mathbb{E}\left[\mathbb{1}_{\{s>\gamma_t(X^\xi)\}}\, K_D(x, X_t^\xi)\, g^\varepsilon(X_s^\xi, s) \right] d\xi\, ds.
\end{aligned}$$

Substituting back gives the full representation for $u(x,t)$. □

4.5 Approximate Representation of u

We now derive an approximate expression for the velocity field $u(x,t)$, based on the stochastic representation of W^ε and the leading-order structure of the source term g^ε. This approximation highlights the dominant contributions from the initial vorticity and the boundary layer dynamics.

Corollary 4.6 (Approximation of u)**.** *Let W^ε solve the boundary value problem equation* (4.2)*, and decompose the vorticity as $\omega = W^\varepsilon + \sigma^\varepsilon$, where $\sigma^\varepsilon(x,t) = \theta(x_1,t)\phi(x_2/\varepsilon)$ is supported near the boundary $x_2 = 0$. Then, under the assumption $\varepsilon \ll 1$, the velocity field admits the approximation*

$$\begin{aligned}
u(x,t) \approx &\int_D \mathbb{E}\left[\mathbb{1}_D(X_t^\xi)\, K_D(X_t^\xi, x) - \mathbb{1}_D(X_t^{\bar{\xi}})\, K_D(X_t^{\bar{\xi}}, x) \right] \omega_0(\xi)\, d\xi \\
&+ \int_0^t \int_D \mathbb{E}\left[\mathbb{1}_{\{s>\gamma_t(X^\xi)\}}\, K_D(X_t^\xi, x)\, G(X_s^\xi, s) \right] d\xi\, ds \\
&+ \frac{\nu}{\varepsilon^2} \int_0^t \int_D \mathbb{E}\left[\mathbb{1}_{\{s>\gamma_t(X^\xi)\}}\, K_D(X_t^\xi, x)\, \theta((X_s^\xi)_1, s)\, \phi''\left(\frac{(X_s^\xi)_2}{\varepsilon} \right) \right] d\xi\, ds. \quad (4.7)
\end{aligned}$$

Proof. Starting from the stochastic representation in Theorem 4.5, we write

$$\begin{aligned} u(x,t) = &\int_D K_D(x,y)\,\sigma^\varepsilon(y,t)\,dy \\ &+ \int_D \mathbb{E}\left[\mathbb{1}_D(X_t^\xi)\,K_D(x,X_t^\xi) - \mathbb{1}_D(X_t^{\bar{\xi}})\,K_D(x,X_t^{\bar{\xi}})\right] W^\varepsilon(\xi,0)\,d\xi \\ &+ \int_0^t \int_D \mathbb{E}\left[\mathbb{1}_{\{s>\gamma_t(X^\xi)\}}\,K_D(x,X_t^\xi)\,g^\varepsilon(X_s^\xi,s)\right]\,d\xi\,ds. \end{aligned}$$

The first term vanishes in the limit $\varepsilon \to 0$ for x away from the boundary, since σ^ε is supported in a thin boundary layer and K_D is smooth there:

$$\int_D K_D(x,y)\,\sigma^\varepsilon(y,t)\,dy \to 0 \quad \text{as } \varepsilon \to 0.$$

For the second term, we use the initial condition $W^\varepsilon(\xi,0) = \omega_0(\xi)$, yielding

$$\int_D \mathbb{E}\left[\mathbb{1}_D(X_t^\xi)\,K_D(x,X_t^\xi) - \mathbb{1}_D(X_t^{\bar{\xi}})\,K_D(x,X_t^{\bar{\xi}})\right]\omega_0(\xi)\,d\xi.$$

For the third term, we use the approximation from equation (4.3):

$$g^\varepsilon(x,t) = G(x,t) + \frac{\nu}{\varepsilon^2}\,\theta(x_1,t)\,\phi''\left(\frac{x_2}{\varepsilon}\right),$$

which contributes the last two terms in equation (4.7). □

Remark. This approximation captures the asymptotic behavior of $u(x,t)$ as $\varepsilon \to 0$, revealing how the boundary layer profile σ^ε and the singular term in g^ε influence the velocity through the Biot–Savart kernel.

4.6 Numerical Scheme for u

We present a numerical method for approximating the velocity field $u(x,t)$, based on the stochastic representation in Theorem 4.6. The scheme combines Monte Carlo simulation of stochastic particle paths with discrete summation over a spatial mesh and time steps.

The domain $D \subset \mathbb{R}^2$ is discretized using a non-uniform grid (i_1, i_2), with finer resolution near the boundary $x_2 = 0$ to capture boundary layer effects. Let A_{i_1,i_2} denote the area element at grid cell (i_1, i_2), and ω_{i_1,i_2} the corresponding initial vorticity value. Define $D_b \subset D$ as the subset of grid indices with $0 < x_2^{(i_2)} < c\varepsilon$, for some constant $c > 0$, to isolate the boundary layer.

For each grid point, let $X_{t_k}^{i_1,i_2}$ denote the position of a simulated particle at time t_k, and let $\gamma_{t_k}(X^{i_1,i_2})$ be the last time the particle touched the boundary before t_k. The

Biot–Savart kernel $K_D(\cdot, x)$ evaluates the contribution to the velocity at the target point $x \in D$.

The velocity field at time t_{k+1} is approximated by

$$\begin{aligned}
&\hat{u}(x, t_{k+1}) = \\
&\sum_{(i_1,i_2)\in D,\, i_2>0} A_{i_1,i_2}\, \omega_{i_1,i_2} \left(\mathbb{1}_D(X_{t_k}^{i_1,i_2}) K_D(X_{t_k}^{i_1,i_2}, x) - \mathbb{1}_D(X_{t_k}^{i_1,-i_2}) K_D(X_{t_k}^{i_1,-i_2}, x) \right) \\
&+ \sum_{(i_1,i_2)\in D} A_{i_1,i_2}\, \Delta t \cdot K_D(X_{t_k}^{i_1,i_2}, x) \sum_{l=0}^{k} \mathbb{1}_{\{t_l > \gamma_{t_k}(X_{t_k}^{i_1,i_2})\}} G_{i_1,i_2;t_l} \\
&+ \frac{\nu}{\varepsilon^2} \sum_{(i_1,i_2)\in D_b} A_{i_1,i_2}\, \Delta t \cdot K_D(X_{t_k}^{i_1,i_2}, x) \sum_{l=0}^{k} \mathbb{1}_{\{t_l > \gamma_{t_k}(X_{t_k}^{i_1,i_2})\}} \theta\left((X_{t_l}^{i_1,i_2})_1, t_l \right) \phi''\left(\frac{(X_{t_l}^{i_1,i_2})_2}{\varepsilon} \right).
\end{aligned} \tag{4.8}$$

The first term approximates the velocity induced by the initial vorticity using the mirrored process identity. The second accumulates the contribution of the external forcing G along trajectories, and the third captures the dominant boundary layer effect from the singular term in g^ε.

The scheme is mesh-free in evaluating $u(x, t)$ at arbitrary points, making it flexible for complex domains. It is also parallelizable, efficient, and well suited to simulating viscous flows in wall-bounded geometries.

4.7 Boundary Vorticity Dynamics

To implement the numerical scheme for u, we require the boundary vorticity profile $\theta(x_1, t) := \omega(x_1, 0, t)$. The following result, adapted from [1], describes its evolution in two-dimensional viscous flows.

Proposition 4.7 (Boundary vorticity evolution)**.** *Let $d = 2$. Then the boundary vorticity $\theta(x_1, t) := \omega(x_1, 0, t)$ satisfies*

$$\frac{\partial \theta}{\partial t} - 2\nu \frac{\partial^2 \theta}{\partial x_1^2} - \nu \left(\frac{\partial}{\partial \eta} \right)^3 u_1 \Big|_{\partial D} - G|_{\partial D} = 0, \tag{4.9}$$

where u_1 is the tangential velocity, η is the outward unit normal to the boundary ∂D, and $G = \nabla \times F$ is the vorticity of the external force.

Proof. In two dimensions, the vorticity is given by

$$\omega = \frac{\partial u_2}{\partial x_1} - \frac{\partial u_1}{\partial x_2}.$$

The vorticity equation reads

$$\frac{\partial \omega}{\partial t} + (u \cdot \nabla)\omega - \nu \Delta \omega = G.$$

We compute the Laplacian:

$$\Delta \omega = \frac{\partial^3 u_2}{\partial x_1^3} - \frac{\partial^3 u_1}{\partial x_1^2 \partial x_2} + \frac{\partial^3 u_2}{\partial x_2^2 \partial x_1} - \frac{\partial^3 u_1}{\partial x_2^3}.$$

Using incompressibility $\nabla \cdot u = 0$, we replace:

$$\frac{\partial^2 u_2}{\partial x_1^2} = -\frac{\partial^3 u_1}{\partial x_1^2 \partial x_2}, \quad \frac{\partial^2 u_2}{\partial x_2^2} = -\frac{\partial^3 u_1}{\partial x_2^3}.$$

Hence,

$$\Delta \omega = 2\frac{\partial^2 \omega}{\partial x_1^2} - \frac{\partial^3 u_2}{\partial x_1^3} - \frac{\partial^3 u_1}{\partial x_2^3}.$$

On the boundary ∂D, we define $\theta(x_1, t) := \omega(x_1, 0, t)$. Assuming $u_2(x_1, 0) = 0$ and that u_2 vanishes smoothly near the wall, we neglect the term $\partial^3_{x_1^3} u_2\big|_{\partial D}$. This gives:

$$\Delta \omega|_{\partial D} = 2\frac{\partial^2 \theta}{\partial x_1^2} + \left(\frac{\partial}{\partial \eta}\right)^3 u_1\Big|_{\partial D}.$$

Substituting into the vorticity equation on the boundary yields equation (4.9). □

Remark. In the case of the upper half-plane, the boundary is the flat wall $\partial D = \{x_2 = 0\}$, and the unit outward normal is $\eta = -\mathbf{e}_2$. Therefore,

$$\frac{\partial}{\partial \eta} = -\frac{\partial}{\partial x_2}, \qquad \psi(x_1, t) := G(x_1, 0, t),$$

and the general boundary vorticity evolution equation (4.9) simplifies to

$$\frac{\partial \theta}{\partial t} - 2\nu \frac{\partial^2 \theta}{\partial x_1^2} = \psi(x_1, t) - \nu \frac{\partial^3 u_1}{\partial x_2^3}(x_1, 0, t). \tag{4.10}$$

We solve this equation to evolve the boundary vorticity $\theta(x_1, t) := \omega(x_1, 0, t)$ in our simulation.

Lemma 4.8 (Duhamel's Principle)**.** *Let L be a second-order linear operator. For the inhomogeneous parabolic equation*

$$\begin{cases} \left(\dfrac{\partial}{\partial t} - L\right) w(x,t) = G(x,t), & x \in \Omega,\ t > 0, \\ w(x,0) = w_0(x), \end{cases} \tag{4.11}$$

if $\Gamma(x,t;\xi,\tau)$ is the fundamental solution of the associated homogeneous problem, then the solution is given by

$$w(x,t) = \int_\Omega \Gamma(x,t;\xi,0)\, w_0(\xi)\, d\xi + \int_0^t \int_\Omega \Gamma(x,t;\xi,\tau)\, G(\xi,\tau)\, d\xi\, d\tau. \tag{4.12}$$

Details of Duhamel's principle and its role in solving linear parabolic PDEs can be found in Evans [5]. Applying Theorem 4.8 to the boundary vorticity equation equation (4.10), we use the 1D heat kernel

$$h(x_1,t;y_1) = \frac{1}{\sqrt{8\pi\nu t}} \exp\left(-\frac{(x_1-y_1)^2}{8\nu t}\right),$$

to obtain the explicit solution:

$$\theta(x_1,t) = \int_{\mathbb{R}} \theta(y_1,0)\, h(x_1,t;y_1)\, dy_1 + \int_0^t \int_{\mathbb{R}} \left[\psi(y_1,s) - \varphi(y_1,s)\right]\, h(x_1,t-s;y_1)\, dy_1\, ds, \tag{4.13}$$

where $\varphi(x_1,t) := \nu\, \partial^3_{x_2} u_1(x_1,x_2,t)\big|_{x_2=0}$.

This has a stochastic representation:

$$\theta(x_1,t) = \mathbb{E}[\theta(X,0)] + \int_0^t \mathbb{E}[\psi(Y^s,s) - \varphi(Y^s,s)]\, ds,$$

where $X \sim \mathcal{N}(x_1, 4\nu t)$ and $Y^s \sim \mathcal{N}(x_1, 4\nu(t-s))$.

Discretizing in time and sampling yields the Monte Carlo estimator:

$$\theta(x_1,t_{k+1}) \approx \frac{1}{N}\sum_{i=1}^N \theta(X_i,0) + \frac{\Delta t}{N}\sum_{i=1}^N \sum_{j=0}^k \left[\psi(Y_i^{t_j},t_j) - \varphi(Y_i^{t_j},t_j)\right], \tag{4.14}$$

where $X_i \sim \mathcal{N}(x_1, 4\nu t_{k+1})$, $Y_i^{t_j} \sim \mathcal{N}(x_1, 4\nu(t_{k+1}-t_j))$.

To evaluate φ, we apply a finite difference stencil at each sample point:

$$\left.\frac{\partial^3 u_1}{\partial x_2^3}\right|_{x_2=0} \approx \frac{-5u_1(0) + 18u_1(\Delta x_2) - 24u_1(2\Delta x_2) + 14u_1(3\Delta x_2) - 3u_1(4\Delta x_2)}{2(\Delta x_2)^3}.$$

This expression is evaluated for each Monte Carlo path at every time step.

4.8 Simulation

We simulate incompressible viscous flow in the upper half-plane domain $D = \{(x_1,x_2) \in \mathbb{R}^2 : x_2 > 0\}$, with viscosity $\nu = 0.1$ and total simulation time $T = 20$. The initial

velocity is set as $u(x_1, x_2, 0) = (-\sin x_2, 0)$, corresponding to vorticity $\omega(x_1, x_2, 0) = \cos x_2$. The time step is $\Delta t = 0.1$, resulting in 200 iterations. The spatial domain $x_1 \in [-6, 6]$, $x_2 \in [0, 6]$ is discretized using a non-uniform grid: within the boundary layer region $x_2 < 0.4$, mesh spacings $h_1 = 0.4$, $h_2 = 0.2$ are used; outside this region, a coarser spacing $h_0 = 0.8$ is adopted. The velocity field is computed via the stochastic vortex method, using Monte Carlo simulation of Taylor diffusion and the Biot–Savart kernel with mollification parameter $\delta = 0.1$. Boundary vorticity θ is updated dynamically using 10 Monte Carlo samples per point, and the third-order normal derivative $\partial^3_{x_2} u_1$ is approximated using a finite difference stencil.

The evolution of streamlines over time is shown in figure 4.1. Initially, the flow exhibits horizontal symmetry and a coherent vortex structure near the wall. As the simulation progresses, vorticity accumulates along the boundary and breaks the symmetry, generating a shear layer and deflecting the vortex upward. By $t = 20$, the flow pattern has significantly deformed, with the primary vortex drifting away from the wall due to the influence of the no-slip condition and viscous diffusion. These dynamics illustrate how boundary vorticity interacts with bulk flow and validate the ability of our stochastic method to capture subtle wall-induced effects.

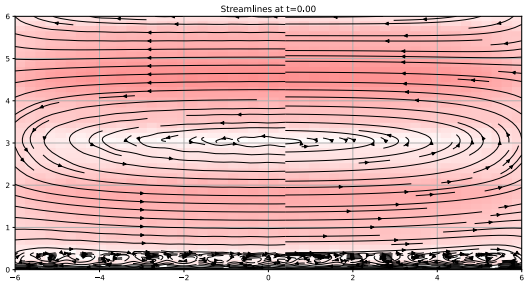

(a) $t = 0$

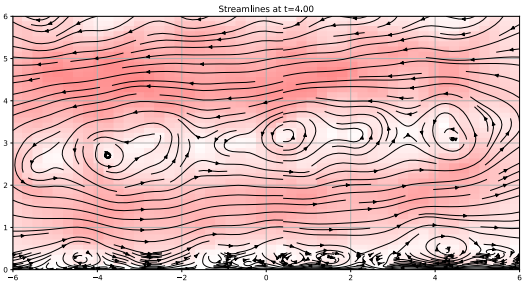

(b) $t = 4$

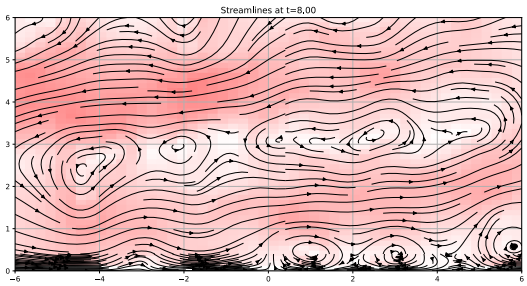

(c) $t = 8$

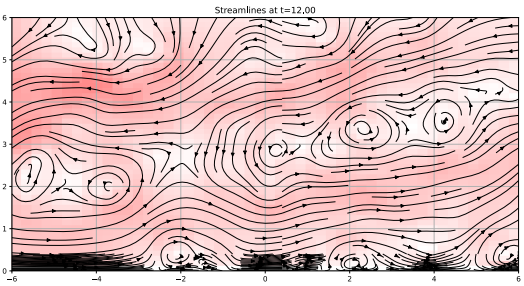

(d) $t = 12$

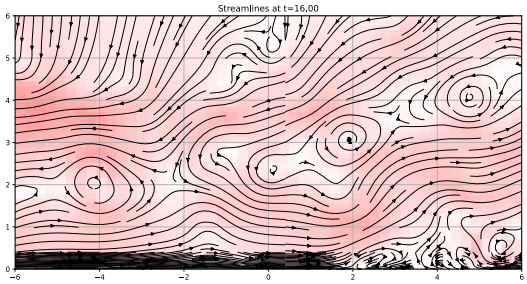

(e) $t = 16$

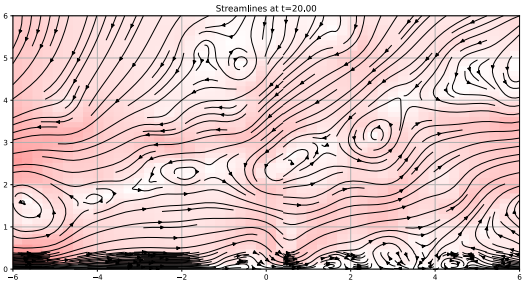

(f) $t = 20$

Figure 4.1: Streamline evolution in the upper half-plane domain $D = \{x_2 > 0\}$, with viscosity $\nu = 0.1$, time step $\Delta t = 0.1$, and final time $T = 20$.

Chapter 5

Flows in Corner Domain

We now extend the analysis from the upper half-plane to the first quadrant domain

$$Q := \{(x_1, x_2) \in \mathbb{R}^2 : x_1 > 0,\ x_2 > 0\},$$

which is bounded by the coordinate axes $\{x_1 = 0\}$ and $\{x_2 = 0\}$. As in the one-wall case, we enforce the no-slip boundary condition using reflection techniques, suitably adapted to account for the presence of two intersecting walls.

To implement the method of images in this setting, we define the following reflections for any point $y = (y_1, y_2) \in \mathbb{R}^2$:

$$\overline{y} := (y_1, -y_2), \qquad \widetilde{y} := (-y_1, y_2), \qquad \overline{\widetilde{y}} := (-y_1, -y_2).$$

These represent reflections across the horizontal axis, the vertical axis, and both axes, respectively.

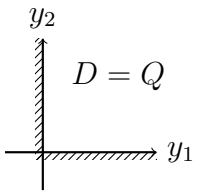

5.1 Biot–Savart Law in the Corner Domain

To derive the Biot–Savart law in the quadrant Q, we first construct a Green's function that satisfies homogeneous Dirichlet boundary conditions on both axes.

Lemma 5.1 (Green's function in the corner domain)**.** *Let $G(t, x; s, y)$ denote the fundamental solution of the heat equation in $\mathbb{R}^2$. Then the Green's function G_Q for*

the heat equation in Q, which vanishes on ∂Q, is given by

$$\begin{aligned} G_Q(s,x;t,y) = G(s,x;t,y) - G(s,x;t,\widetilde{y}) \\ - G(s,x;t,\overline{y}) + G(s,x;t,\overline{\widetilde{y}}), \end{aligned} \tag{5.1}$$

for all $x, y \in Q$ and $s < t$.

Remark. This formula follows from the method of images. The reflection $y \mapsto \widetilde{y}$ enforces the vanishing condition on the vertical boundary $\{x_1 = 0\}$, while the reflection $y \mapsto \overline{y}$ imposes the same on the horizontal boundary $\{x_2 = 0\}$. The final correction term involving $\overline{\widetilde{y}}$ guarantees cancellation at the corner point. This generalizes the one-wall construction in Theorem 4.1.

Lemma 5.2 (Biot–Savart kernel in the corner domain)**.** *The Biot–Savart kernel in the quadrant Q, which yields a velocity field $u = K_Q * \omega$ satisfying $u|_{\partial Q} = 0$, is given by*

$$K_Q(x,y) = \left(K_{1,Q}(x,y),\ K_{2,Q}(x,y)\right),$$

where

$$\begin{aligned} K_{1,Q}(x,y) &= -\frac{1}{2\pi}\left[\frac{x_2-y_2}{|x-y|^2} - \frac{x_2-y_2}{|x-\widetilde{y}|^2} - \frac{x_2+y_2}{|x-\overline{y}|^2} + \frac{x_2+y_2}{|x-\overline{\widetilde{y}}|^2}\right], \\ K_{2,Q}(x,y) &= \frac{1}{2\pi}\left[\frac{x_1-y_1}{|x-y|^2} - \frac{x_1+y_1}{|x-\widetilde{y}|^2} - \frac{x_1-y_1}{|x-\overline{y}|^2} + \frac{x_1+y_1}{|x-\overline{\widetilde{y}}|^2}\right]. \end{aligned}$$

Remark. This kernel is derived by differentiating the Green's function G_Q from Theorem 5.1, following the same procedure used in the unbounded domain (see Theorem 3.3) and in the upper half-plane (see the corollary following Theorem 4.1). The reflected terms ensure both the tangential and normal velocity components vanish on the boundaries, thereby enforcing the no-slip condition on ∂Q.

5.2 Boundary Layer Correction

To enforce homogeneous Dirichlet boundary conditions on both walls of the quadrant domain $Q = \{x_1 > 0,\ x_2 > 0\}$, we introduce a boundary layer correction analogous to the one-wall case, now extended to handle the presence of two intersecting boundaries.

Let $\phi \in C^2([0,\infty))$ denote the same smooth cutoff function used in the upper half-plane analysis, compactly supported in $[0, 2/3]$, with $\phi(0) = 1$, $\phi(r) = 0$ for $r \geq 2/3$, and explicitly defined derivatives ϕ', ϕ'' as before.

We define the boundary vorticity traces along the walls:

$$\theta^x(x_1,t) := \omega(x_1,0,t), \qquad \theta^y(x_2,t) := \omega(0,x_2,t),$$

and construct mollified boundary layer corrections:

$$\sigma_x^\varepsilon(x_1, x_2, t) = \theta^x(x_1, t)\,\phi\left(\frac{x_2}{\varepsilon}\right),$$
$$\sigma_y^\varepsilon(x_1, x_2, t) = \theta^y(x_2, t)\,\phi\left(\frac{x_1}{\varepsilon}\right).$$

We define the boundary-corrected vorticity by

$$W^\varepsilon(x,t) := \omega(x,t) - \sigma_x^\varepsilon(x,t) - \sigma_y^\varepsilon(x,t),$$

which satisfies $W^\varepsilon|_{\partial Q} = 0$. This transformation reduces the original inhomogeneous boundary value problem to a homogeneous one, enabling the use of the Green's function G_Q from Theorem 5.1 and corresponding stochastic representation techniques.

Substituting W^ε into the vorticity transport equation

$$\left(\frac{\partial}{\partial t} + u\cdot\nabla - \nu\Delta\right)\omega = G,$$

yields the following evolution equation for W^ε:

$$\left(\frac{\partial}{\partial t} + u\cdot\nabla - \nu\Delta\right)W^\varepsilon = g^\varepsilon(x,t), \qquad W^\varepsilon|_{\partial Q} = 0, \tag{5.2}$$

where the residual source term g^ε is given by:

$$\begin{aligned}
g^\varepsilon(x,t) &= G(x,t) + \left(\frac{\partial}{\partial t} + u\cdot\nabla - \nu\Delta\right)(\sigma_x^\varepsilon + \sigma_y^\varepsilon) \\
&= G + \frac{\nu}{\varepsilon^2}\phi''\left(\frac{x_2}{\varepsilon}\right)\theta^x(x_1,t) + \frac{\nu}{\varepsilon^2}\phi''\left(\frac{x_1}{\varepsilon}\right)\theta^y(x_2,t) \\
&\quad - \frac{1}{\varepsilon}\phi'\left(\frac{x_2}{\varepsilon}\right)u_2(x,t)\theta^x(x_1,t) - \frac{1}{\varepsilon}\phi'\left(\frac{x_1}{\varepsilon}\right)u_1(x,t)\theta^y(x_2,t) \\
&\quad + \phi\left(\frac{x_2}{\varepsilon}\right)\left[\nu\partial_{x_1}^2\theta^x(x_1,t) - \partial_t\theta^x(x_1,t) - u_1(x,t)\partial_{x_1}\theta^x(x_1,t)\right] \\
&\quad + \phi\left(\frac{x_1}{\varepsilon}\right)\left[\nu\partial_{x_2}^2\theta^y(x_2,t) - \partial_t\theta^y(x_2,t) - u_2(x,t)\partial_{x_2}\theta^y(x_2,t)\right].
\end{aligned} \tag{5.3}$$

As in the one-wall case (see equation (4.3)), the dominant contributions in g^ε come from the second derivative terms involving ϕ'', scaled by ν/ε^2, representing strong diffusion effects localized near the boundaries. The ϕ'-dependent terms capture advection of the boundary vorticity, while the remaining terms govern tangential evolution along the walls.

Remark. All components of g^ε are confined to thin $O(\varepsilon)$-neighborhoods of the coordinate axes due to the compact support of ϕ, ϕ', and ϕ''. Moreover, the no-slip boundary condition implies that the velocity components u_1 and u_2 vanish on ∂Q and remain small nearby. Hence, to leading order, we may approximate:

$$g^\varepsilon(x,t) \approx G(x,t) + \frac{\nu}{\varepsilon^2}\phi''\left(\frac{x_2}{\varepsilon}\right)\theta^x(x_1,t) + \frac{\nu}{\varepsilon^2}\phi''\left(\frac{x_1}{\varepsilon}\right)\theta^y(x_2,t) + O(\varepsilon).$$

5.3 Approximation Formula for u

We now derive an approximation formula for the velocity field $u(x,t)$ in the corner domain Q, using stochastic representations and the symmetry properties of the heat equation. The key idea is to extend the method of mirror processes, previously used in the upper half-plane case, to accommodate two intersecting boundaries via reflections across both coordinate axes.

Recall the mirrored points $\overline{\xi}$, $\widetilde{\xi}$, and $\overline{\widetilde{\xi}}$ introduced earlier. These represent reflections across the horizontal, vertical, and both axes, respectively.

Lemma 5.3 (Mirrored Expectation Identity in the Corner Domain)**.** *Let $f : \mathbb{R}^2 \to \mathbb{R}$ be any bounded measurable function. Then, for the stochastic process X_t^ξ with killing time $\zeta(X^\xi)$, the following identity holds:*

$$\begin{aligned}\mathbb{E}\left[\mathbb{1}_{\{\zeta(X^\xi)>t\}} f(X_t^\xi)\right] &= \mathbb{E}\left[\mathbb{1}_Q(X_t^\xi) f(X_t^\xi)\right] - \mathbb{E}\left[\mathbb{1}_Q(X_t^{\overline{\xi}}) f(X_t^{\overline{\xi}})\right] \\ &\quad - \mathbb{E}\left[\mathbb{1}_Q(X_t^{\widetilde{\xi}}) f(X_t^{\widetilde{\xi}})\right] + \mathbb{E}\left[\mathbb{1}_Q(X_t^{\overline{\widetilde{\xi}}}) f(X_t^{\overline{\widetilde{\xi}}})\right]. \qquad (5.4)\end{aligned}$$

Remark. This identity generalizes Theorem 4.4 from the one-wall setting. It arises by applying the method of images to the heat kernel, which remains symmetric under coordinate mirroring. This formulation captures the joint influence of both boundaries and allows us to represent expectations conditioned on survival within the corner domain.

We now use this result to derive a stochastic approximation of the velocity field, incorporating contributions from the initial vorticity, external forcing, and boundary layers. Using the Biot–Savart kernel K_Q defined in Theorem 5.2, we obtain the following approximation.

Corollary 5.4 (Velocity Approximation in the Corner Domain)**.** *The velocity field $u(x,t)$ in the quadrant domain Q can be approximated by:*

$$\begin{aligned}u(x,t) \approx &\int_Q \mathbb{E}\left[K_Q(X_t^\xi, x) - K_Q(X_t^{\overline{\xi}}, x) - K_Q(X_t^{\widetilde{\xi}}, x) + K_Q(X_t^{\overline{\widetilde{\xi}}}, x)\right] \omega_0(\xi)\, d\xi \\ &+ \int_0^t \int_Q \mathbb{E}\left[\mathbb{1}_{\{s>\gamma_t(X^\xi)\}} K_Q(X_t^\xi, x)\, G(X_s^\xi, s)\right] d\xi\, ds \\ &+ \frac{\nu}{\varepsilon^2} \int_0^t \int_Q \mathbb{E}\left[\mathbb{1}_{\{s>\gamma_t(X^\xi)\}} K_Q(X_t^\xi, x)\, \theta^y((X_s^\xi)_2, s)\, \phi''\left(\frac{(X_s^\xi)_1}{\varepsilon}\right)\right] d\xi\, ds \\ &+ \frac{\nu}{\varepsilon^2} \int_0^t \int_Q \mathbb{E}\left[\mathbb{1}_{\{s>\gamma_t(X^\xi)\}} K_Q(X_t^\xi, x)\, \theta^x((X_s^\xi)_1, s)\, \phi''\left(\frac{(X_s^\xi)_2}{\varepsilon}\right)\right] d\xi\, ds. \qquad (5.5)\end{aligned}$$

Proof. We begin with the decomposition of the vorticity field $\omega = W^\varepsilon + \sigma_x^\varepsilon + \sigma_y^\varepsilon$, and apply the Biot–Savart law:

$$u(x,t) = \int_Q K_Q(x,y)\,\omega(y,t)\,dy = \int_Q K_Q(x,y)\,W^\varepsilon(y,t)\,dy + \int_Q K_Q(x,y)\,(\sigma_x^\varepsilon + \sigma_y^\varepsilon)(y,t)\,dy.$$

The second term captures the effect of the boundary layer corrections. Since both σ_x^ε and σ_y^ε are supported near ∂Q, the leading-order contribution is localized and approximated using the mollifier ϕ'', resulting in the final two terms of the formula.

To handle the term involving W^ε, we invoke Theorem 4.3, which expresses W^ε via expectations over stochastic trajectories surviving up to time t. Substituting this into the Biot–Savart law and interchanging integrals, we obtain:

$$\int_Q K_Q(x,y)\,W^\varepsilon(y,t)\,dy \tag{5.6}$$

$$= \int_Q \int_Q K_Q(x,y)\,\mathbb{E}\left[\mathbb{1}_{\{\zeta(X^\xi)>t\}}\,W^\varepsilon(\xi,0)\,\middle|\,X_t^\xi = y\right] p(0,\xi;t,y)\,d\xi\,dy$$
$$+ \int_0^t \int_Q \int_Q K_Q(x,y)\,\mathbb{E}\left[\mathbb{1}_{\{s>\gamma_t(X^\xi)\}}\,g^\varepsilon(X_s^\xi,s)\,\middle|\,X_t^\xi = y\right] p(0,\xi;t,y)\,d\xi\,dy\,ds. \tag{5.7}$$

We apply Theorem 5.3 to express the conditional expectations as reflected trajectories in Q. This transformation reduces the problem to evaluating expectations of $K_Q(X_t^\xi, x)$ with initial data and source terms along stochastic paths.

Finally, by substituting the dominant components of g^ε from equation (5.3) and neglecting subleading advection and tangential terms, we arrive at the stated approximation. □

Remark. This result mirrors the velocity representation in the upper half-plane, with additional mirrored processes to enforce boundary conditions in the corner. The first line captures the influence of the initial vorticity, the second represents internal forcing, and the last two account for boundary layer corrections along the vertical and horizontal walls. The kernel K_Q ensures that the velocity field satisfies $u|_{\partial Q} = 0$.

5.4 Numerical Scheme for u

We approximate the velocity field $u(x, t_{k+1})$ using the stochastic representation in Theorem 5.4, replacing integrals with quadrature over a spatial grid $(i_1, i_2) \in Q$ and

expectations with Monte Carlo sampling. The scheme reads:

$$
\begin{aligned}
&\hat{u}(x,t_{k+1}) = \\
&\sum_{(i_1,i_2)\in Q} A_{i_1,i_2}\omega_{i_1,i_2}\Big(\mathbb{1}_Q(X_{t_k}^{i_1,i_2})K_Q(X_{t_k}^{i_1,i_2},x) - \mathbb{1}_Q(X_{t_k}^{i_1,-i_2})K_Q(X_{t_k}^{i_1,-i_2},x) \\
&\qquad - \mathbb{1}_Q(X_{t_k}^{-i_1,i_2})K_Q(X_{t_k}^{-i_1,i_2},x) + \mathbb{1}_Q(X_{t_k}^{-i_1,-i_2})K_Q(X_{t_k}^{-i_1,-i_2},x)\Big) \\
&+ \sum_{(i_1,i_2)\in Q} A_{i_1,i_2}\Delta t\cdot K_Q(X_{t_k}^{i_1,i_2},x)\sum_{l=0}^{k}\mathbb{1}_{\{t_l>\gamma_{t_k}(X_{t_k}^{i_1,i_2})\}}\,G_{i_1,i_2;t_l} \\
&+ \frac{\nu}{\varepsilon^2}\sum_{(i_1,i_2)\in Q_{b_x}\cup Q_{b_{xy}}} A_{i_1,i_2}\Delta t\cdot K_Q(X_{t_k}^{i_1,i_2},x)\sum_{l=0}^{k}\mathbb{1}_{\{t_l>\gamma_{t_k}(X_{t_k}^{i_1,i_2})\}}\,\theta^x((X_{t_l}^{i_1,i_2})_1,t_l)\phi''\left(\frac{(X_{t_l}^{i_1,i_2})_2}{\varepsilon}\right) \\
&+ \frac{\nu}{\varepsilon^2}\sum_{(i_1,i_2)\in Q_{b_y}\cup Q_{b_{xy}}} A_{i_1,i_2}\Delta t\cdot K_Q(X_{t_k}^{i_1,i_2},x)\sum_{l=0}^{k}\mathbb{1}_{\{t_l>\gamma_{t_k}(X_{t_k}^{i_1,i_2})\}}\,\theta^y((X_{t_l}^{i_1,i_2})_2,t_l)\phi''\left(\frac{(X_{t_l}^{i_1,i_2})_1}{\varepsilon}\right).
\end{aligned}
\tag{5.8}
$$

Here, A_{i_1,i_2} denotes the quadrature weight, $G_{i_1,i_2;t_l}$ the external forcing, and $\gamma_{t_k}(X)$ the last boundary hit time before t_k. Boundary layer corrections are applied in the near-wall regions Q_{b_x}, Q_{b_y}, and $Q_{b_{xy}}$.

Remark. The wall vorticity traces $\theta^x(x_1,t) := \omega(x_1,0,t)$ and $\theta^y(x_2,t) := \omega(0,x_2,t)$ are computed stochastically using the Duhamel equation (4.14), derived from the boundary vorticity equation (4.10). Each trace evolves independently along the corresponding axis, with the third-order normal derivative estimated via finite differences.

5.5 Simulation

We simulate viscous incompressible flow in the corner domain $Q = [0,8]^2$, with viscosity $\nu = 0.1$. A nonuniform Cartesian mesh is employed: the bulk is discretized with spacing $h_0 = 0.8$, while finer grids with $h_1 = 0.4$ and $h_2 = 0.2$ are used in the near-wall regions Q_{b_x}, Q_{b_y}, and $Q_{b_{xy}}$, defined within a boundary layer width $\delta = 0.8$. The initial velocity field is given by

$$u(x,y) = \frac{-1}{\sqrt{2}}\sin\left(\frac{1}{\sqrt{2}}(y-x)\right)(1,1),$$

corresponding to the vorticity $\omega(x,y) = \cos\left(\frac{1}{\sqrt{2}}(y-x)\right)$. The flow is evolved using Euler–Maruyama time-stepping with $\Delta t = 0.1$ up to final time $T = 20$.

The velocity field is reconstructed from vorticity via the mollified Biot–Savart kernel K_Q^δ with smoothing parameter $\delta = 0.1$. Boundary layer contributions from

wall vorticity traces θ^x and θ^y are included using the stochastic Duhamel formulation equation (4.14), computed through Monte Carlo sampling along the respective coordinate axes.

Figure 5.1 displays streamline plots at selected times. The flow forms interior circulation zones and develops thin shear layers near the walls. As time progresses, viscous diffusion and boundary interactions accumulate, distorting the initial symmetry. Notably, small-scale turbulence emerges near the bottom boundary, illustrating complex interactions between boundary layers and bulk dynamics.

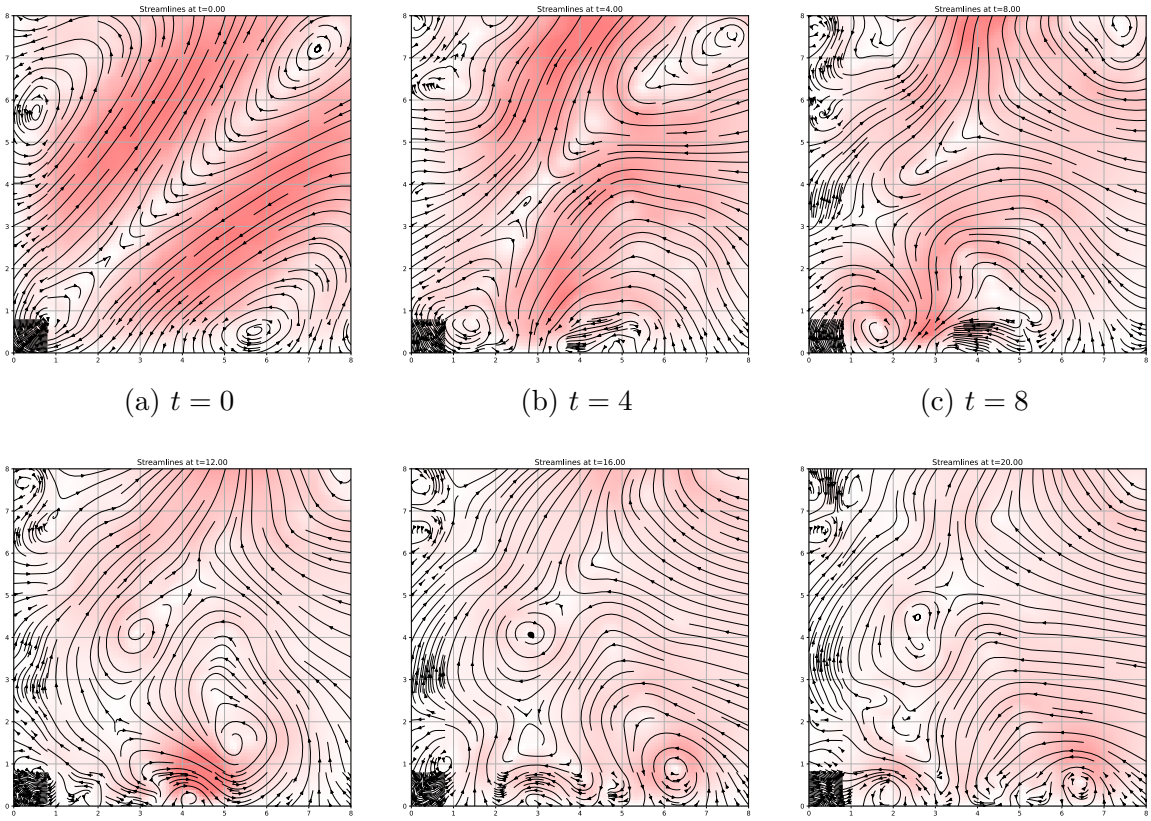

(a) $t = 0$ (b) $t = 4$ (c) $t = 8$

(d) $t = 12$ (e) $t = 16$ (f) $t = 20$

Figure 5.1: Streamline evolution in the corner domain $Q = \{x_1 > 0,\ x_2 > 0\}$, with viscosity $\nu = 0.1$, time step $\Delta t = 0.1$, and final time $T = 20$.

Chapter 6

Flows in Belt Domain

We now consider incompressible viscous flow in a belt-like domain bounded by two parallel walls. Specifically, we define the domain

$$D := \Omega_{\text{belt}} := \{(y_1, y_2) \in \mathbb{R}^2 : 0 < y_2 < a\},$$

where the velocity field must satisfy the no-slip boundary condition along both horizontal boundaries $y_2 = 0$ and $y_2 = a$.

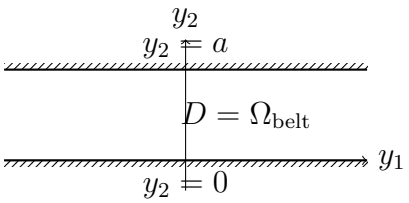

6.1 Biot–Savart

To enforce the Dirichlet boundary condition $u|_{\partial D} = 0$, we construct a Green's function that vanishes on both horizontal boundaries using the method of images.

Lemma 6.1 (Green's function in the belt domain)**.** *Let $G(x, y, t)$ be the fundamental solution of the heat equation in $\mathbb{R}^2$. Then the Dirichlet Green's function for the belt domain $D = \{y \in \mathbb{R}^2 : 0 < y_2 < a\}$ is*

$$G_{\text{belt}}(x, y, t) = \sum_{n \in \mathbb{Z}} \left[G\big(x, (y_1, y_2 + 2an), t\big) - G\big(x, (y_1, -y_2 + 2an), t\big) \right], \tag{6.1}$$

which vanishes on $y_2 = 0$ and $y_2 = a$.

Remark. Reflections across the walls $y_2 = 0$ and $y_2 = a$ generate image sources that cancel boundary flux. The alternating signs ensure Dirichlet conditions. Unlike the one-wall or corner cases, this requires infinitely many reflections.

Differentiating G_{belt} with respect to y yields the Biot–Savart kernel that maps vorticity to velocity:

Lemma 6.2 (Biot–Savart law in the belt domain)**.** *Let $x, y \in D$, and define*

$$K(x,y) := (K_{1,\text{belt}}(x,y),\, K_{2,\text{belt}}(x,y))$$

with components

$$K_{1,\text{belt}}(x,y) = -\frac{1}{2\pi}\sum_{n\in\mathbb{Z}}\left[\frac{x_2-(y_2+2an)}{|x-(y_1,y_2+2an)|^2} - \frac{x_2-(-y_2+2an)}{|x-(y_1,-y_2+2an)|^2}\right],$$
$$K_{2,\text{belt}}(x,y) = \frac{1}{2\pi}\sum_{n\in\mathbb{Z}}\left[\frac{x_1-y_1}{|x-(y_1,y_2+2an)|^2} - \frac{x_1-y_1}{|x-(y_1,-y_2+2an)|^2}\right].$$

Then the velocity field is reconstructed by

$$u(x,t) = \int_D K(x,y)\, w(y,t)\, dy.$$

Remark. This kernel is obtained by differentiating the alternating sum of image sources in the Green's function. Unlike the upper half-plane or corner domains, where reflection symmetry allows closed-form expressions with finitely many terms, the belt geometry lacks such symmetry and requires *infinitely many reflections* to enforce vanishing conditions on both walls. The series converges rapidly when x_2 and y_2 are far from the boundaries, but its infinite nature presents a computational obstacle.

Since we cannot establish mirror lemmas analogous to those used in the half-plane or corner cases (e.g. Theorem 4.4 and Theorem 5.3), stochastic representations involving reflected Brownian motion are no longer available. In particular, the absence of a corresponding expectation identity prevents us from directly applying the method of images. To evaluate the velocity field probabilistically while respecting boundary conditions, we instead introduce an *extended velocity formulation* combined with a *boundary-layer perturbation*, as developed in the following subsections.

6.2 Extended velocity field

In the upper half-plane and corner domains, the reflection principle enables the construction of stochastic representations that satisfy boundary conditions via reflected Brownian paths. However, this approach breaks down in the belt geometry, where two

parallel walls generate infinitely many reflections. As a result, neither exact Green's functions nor reflected particle trajectories are practical for computation.

To retain a stochastic framework, we extend the velocity field u to the whole plane by

$$u(x,t) := \begin{cases} u(x,t), & x \in D, \\ 0, & x \notin D, \end{cases}$$

so that u remains compactly supported and compatible with no-slip boundaries. The particle motion is then described by

$$\mathrm{d}X_t = \mathbb{1}_D(X_t)\, u(X_t,t)\mathrm{d}t + \sqrt{2\nu}\,\mathrm{d}B_t, \tag{6.2}$$

where B_t is standard Brownian motion. Inside D, the velocity contributes to the drift; outside D, particles diffuse freely.

This formulation enables simulation, but introduces a problem: Brownian motion may exit D, causing errors near boundaries and violating the physical constraints. In particular, the representation

$$w(y,t) = \int_{\mathbb{R}^2} p(0,\xi,t,y)\, w_0(\xi)\, d\xi$$

is no longer valid, as it includes nonphysical contributions from outside the domain.

To address this, we introduce a boundary-layer perturbation. The vorticity is decomposed into an interior part W^ε, treated by particle methods, and a near-wall correction σ^ε, handled analytically. This allows us to approximate $u(x,t)$ while respecting boundary conditions and avoiding unphysical trajectories.

6.3 Velocity evaluation via perturbation decomposition

Due to the failure of the reflection principle in the belt domain, Brownian particles simulated via the extended velocity field may exit the domain, making direct use of stochastic representations inaccurate near the boundaries. To address this, we decompose the vorticity into an interior regularized part and a boundary-layer correction.

Define the regularized vorticity

$$\begin{aligned} W^\varepsilon(x,t) &:= w(x,t) - w(x_1,0,t)\,\phi\left(\frac{x_2}{\varepsilon}\right) - w(x_1,a,t)\,\phi\left(\frac{a-x_2}{\varepsilon}\right) \\ &= w(x,t) - \sigma^\varepsilon(x,t), \end{aligned} \tag{6.3}$$

where ϕ is a smooth cutoff function supported near zero. By construction, $W^\varepsilon(x,t) = 0$ on the boundary, so it may be accurately approximated using random vortex methods without violating the no-slip condition. The subtracted term σ^ε isolates the near-boundary contribution.

Let us write $K := K_{\text{belt}}$. Then we evaluate the velocity via the Biot–Savart law:

$$\begin{aligned}
u(x,t) &= \int_D K(x,y)\, w(y,t)\, dy \\
&= \int_D K(x,y) \left[W^\varepsilon(y,t) + \sigma^\varepsilon(y,t) \right] dy \\
&= \int_D K(x,y)\, W^\varepsilon(y,t)\, dy + \int_D K(x,y)\, \sigma^\varepsilon(y,t)\, dy \\
&= \int_D K(x,y) \left[\int_{\mathbb{R}^2} p(0,\xi,t,y)\, W_0^\varepsilon(\xi)\, d\xi \right] dy + \int_D K(x,y)\, \sigma^\varepsilon(y,t)\, dy \\
&= \int_{\mathbb{R}^2} \left[\int_D K(x,y)\, p(0,\xi,t,y)\, dy \right] W_0^\varepsilon(\xi)\, d\xi + \int_D K(x,y)\, \sigma^\varepsilon(y,t)\, dy \\
&= \int_{\mathbb{R}^2} \mathbb{E}\left[K(x, X_t^\xi) \right] W_0^\varepsilon(\xi)\, d\xi + \int_D K(x,y)\, \sigma^\varepsilon(y,t)\, dy \\
&\approx \int_{\mathbb{R}^2} K(X_t^\xi, x)\, W_0^\varepsilon(\xi)\, d\xi + \int_D K(x,y)\, \sigma^\varepsilon(y,t)\, dy \\
&=: \text{(A)} + \text{(B)}.
\end{aligned} \tag{6.4}$$

The first term (A) represents the contribution from the regularized interior vorticity, which satisfies homogeneous Dirichlet boundary conditions. It is approximated using the random vortex method, where the velocity is reconstructed from simulated particle trajectories governed by the extended velocity field.

Here, W_0^ε is the regularized initial vorticity corresponding to W^ε, given by

$$W_0^\varepsilon(x_1,x_2) = w_0(x_1,x_2) - w_0(x_1,0)\, \phi\left(\frac{x_2}{\varepsilon}\right) - w_0(x_1,a)\, \phi\left(\frac{a-x_2}{\varepsilon}\right). \tag{6.5}$$

This mollified initial data vanishes near both boundaries, so the solution $W^\varepsilon(x,t)$ remains zero on ∂D for all time. Consequently, its evolution is well-described by the Dirichlet heat kernel, and the particle-based representation in (A) is valid. Although W_0^ε is supported only in D, we write the integral over $\mathbb{R}^2$ because the Brownian paths evolve in the full space. In practice, the expectation in (A) is approximated by Monte Carlo sampling and omitted from the notation.

The second term (B) is the correction introduced to recover the influence of vorticity near the walls, which was artificially removed by the subtraction of σ^ε. It is evaluated analytically as

$$\int_D K(x,y)\, w(y_1,0,t)\, \phi\left(\frac{y_2}{\varepsilon}\right) dy + \int_D K(x,y)\, w(y_1,a,t)\, \phi\left(\frac{a-y_2}{\varepsilon}\right) dy,$$

where the boundary vorticities

$$\theta_0(y_1,t) := w(y_1,0,t), \qquad \theta_1(y_1,t) := w(y_1,a,t)$$

are computed from heat-type equations on the respective walls using a Monte Carlo method.

In the presence of external forcing G, the vorticity equation includes a source term, which must also be modified to account for the boundary-layer subtraction. The effective forcing becomes

$$g_\varepsilon(x_1,x_2,t) \approx G(x_1,x_2,t) - \frac{\nu}{\varepsilon^2}\left[\theta_0(x_1,t)\,\phi''\left(\frac{x_2}{\varepsilon}\right) + \theta_1(x_1,t)\,\phi''\left(\frac{a-x_2}{\varepsilon}\right)\right], \quad (6.6)$$

where the correction terms are sharply localized near the boundaries due to the second derivatives of the mollifier. These singular components compensate for the missing wall vorticity, thereby restoring consistency with the no-slip condition at both boundaries.

6.4 Boundary Vorticity Evolution Equation

To complete the velocity evaluation via boundary-layer decomposition, we must compute the boundary vorticity

$$\theta_0(y_1,t) := w(y_1,0,t), \qquad \theta_1(y_1,t) := w(y_1,a,t),$$

which appear in both the correction term σ^ε and the modified forcing g_ε. These quantities evolve according to effective one-dimensional equations derived from restricting the vorticity dynamics to the walls.

We first define the following auxiliary functions:

$$\psi_0(y_1,t) := G(y_1,0,t), \qquad \psi_1(y_1,t) := G(y_1,a,t),$$
$$\varphi_0(y_1,t) := \nu\left.\frac{\partial^3 u^1}{\partial y_2^3}\right|_{y_2=0}, \qquad \varphi_1(y_1,t) := \nu\left.\frac{\partial^3 u^1}{\partial y_2^3}\right|_{y_2=a},$$

where G denotes the external forcing, and φ_i represents the shear-induced vorticity flux at the boundary, associated with the third derivative of the horizontal velocity component u^1.

Then, θ_0 and θ_1 satisfy heat-type equations with source terms, analogous to the one-wall case in equation (4.10):

$$\frac{\partial\theta_0}{\partial t}(y_1,t) - 2\nu\,\frac{\partial^2\theta_0}{\partial y_1^2}(y_1,t) = \psi_0(y_1,t) - \varphi_0(y_1,t), \quad (6.7)$$

$$\frac{\partial\theta_1}{\partial t}(y_1,t) - 2\nu\,\frac{\partial^2\theta_1}{\partial y_1^2}(y_1,t) = \psi_1(y_1,t) - \varphi_1(y_1,t). \quad (6.8)$$

For numerical implementation, we approximate these equations using a Monte Carlo scheme based on the Duhamel formula. At time t_k, the boundary vorticity $\theta_i(x_1, t_k)$ is estimated as

$$\theta_i(x_1, t_k) \approx \frac{1}{N}\sum_{j=1}^{N}\theta_i(X_j, 0) + \frac{\Delta t}{N}\sum_{j=1}^{N}\sum_{l=0}^{k-1}\left[\psi_i(Y_j^l, t_l) - \varphi_i(Y_j^l, t_l)\right], \qquad i = 0, 1, \quad (6.9)$$

where $X_j \sim \mathcal{N}(x_1, 4\nu t_k)$ and $Y_j^l \sim \mathcal{N}(x_1, 4\nu t_l)$ are sampled from one-dimensional Gaussians along the wall.

The shear terms φ_i, involving third-order derivatives in y_2, are approximated using finite difference stencils. Let h denote the vertical grid spacing near the wall. Then:

$$\begin{aligned}
\varphi_0(y_1, t) &\approx \nu\,\frac{-u^1(y_1, 3h, t) + 3u^1(y_1, 2h, t) - 3u^1(y_1, h, t) + u^1(y_1, 0, t)}{h^3}, \\
\varphi_1(y_1, t) &\approx \nu\,\frac{-u^1(y_1, a-3h, t) + 3u^1(y_1, a-2h, t) - 3u^1(y_1, a-h, t) + u^1(y_1, a, t)}{h^3}.
\end{aligned} \quad (6.10)$$

This completes the construction of the boundary vorticity dynamics necessary for evaluating the full velocity field. The wall terms are updated independently of the interior simulation, ensuring that near-wall behavior is accurately captured and incorporated into the perturbation-based framework.

6.5 Simulation

We simulate incompressible viscous flow in the belt domain $D = [-6, 6] \times [0, 6]$, using the random vortex method with boundary-layer correction. The initial velocity field

$$u_0(x, y) = \left(-\frac{1}{2}\sin\left(\frac{2\pi y}{a}\right), 0\right)$$

satisfies the no-slip condition and induces the corresponding vorticity

$$w_0(x, y) = \frac{\pi}{a}\cos\left(\frac{2\pi y}{a}\right).$$

The simulation employs a nonuniform Cartesian mesh with vertical spacing $h_2 = 0.3$ near the walls and $h_0 = 0.8$ in the interior, along with horizontal spacing $h_1 = 0.6$. The boundary-layer thickness is set to $\varepsilon = 0.8$. Time integration is performed up to $T = 20$ using the Euler–Maruyama method with time step $\Delta t = 0.1$ and viscosity $\nu = 0.05$. At each step, $N = 200$ particles are used to approximate interior velocity via stochastic trajectories, while the boundary vorticities θ_0 and θ_1 evolve according

to one-dimensional heat equations, with shear terms approximated using third-order finite difference stencils.

The simulation results are shown in figure 6.1. The streamline plots illustrate how viscous diffusion and wall confinement shape the evolution of the flow. Initially symmetric structures gradually deform as vorticity spreads and interacts with the boundaries. The perturbation-based correction successfully enforces the no-slip condition, producing smooth and stable velocity fields. Vorticity accumulates near the walls and gradually redistributes across the domain, with streamline elongation and flattening consistent with viscous damping effects.

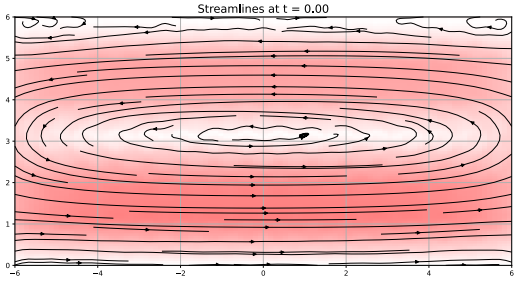

(a) $t = 0$

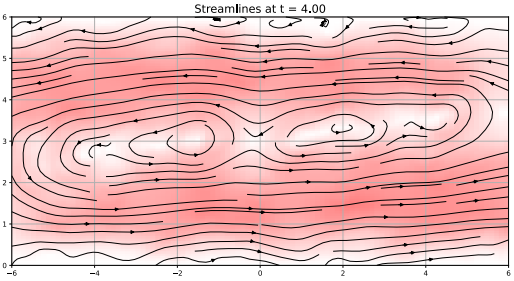

(b) $t = 4$

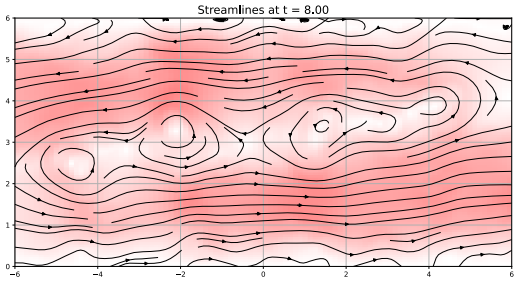

(c) $t = 8$

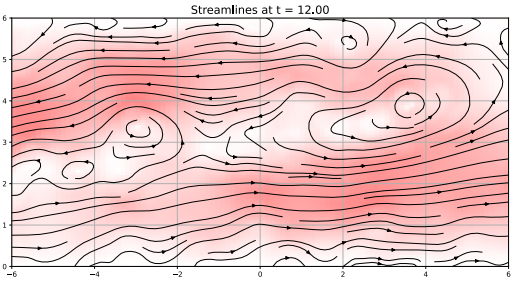

(d) $t = 12$

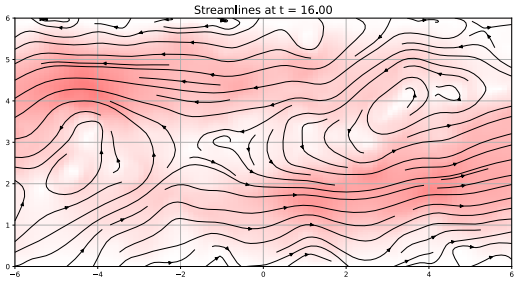

(e) $t = 16$

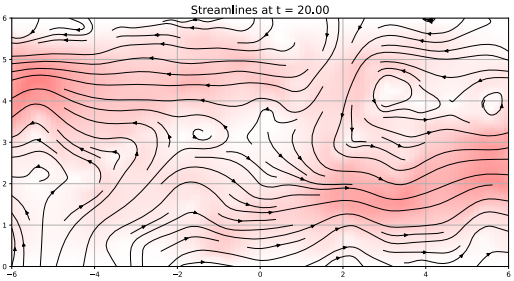

(f) $t = 20$

Figure 6.1: Streamline evolution in the belt domain $D = \mathbb{R} \times [0, 6]$, with viscosity $\nu = 0.05$, time step $\Delta t = 0.1$, and final time $T = 20$.

Chapter 7

Discussion

This dissertation develops the random vortex method for the two-dimensional incompressible Navier–Stokes equations across four domains: the unbounded plane, the upper half-plane, the corner domain, and the belt domain. The unbounded case (Chapter 3) follows classical formulations [3, 6, 9], while the upper half-plane setting (Chapter 4) builds on recent stochastic representations for wall-bounded flows [12, 1]. In contrast, the treatments for the corner domain (Chapter 5) and belt domain (Chapter 6) constitute original contributions. For the corner case, we construct a novel reflection-based Biot–Savart kernel and design tailored boundary vorticity corrections. For the belt domain, we introduce a formulation involving infinite image summation, an extended velocity decomposition, and a perturbation-based correction. These extensions highlight the adaptability of the probabilistic vortex framework to more intricate boundary geometries.

Although the upper half-plane formulation builds upon existing techniques [12, 1], extending the method to multiply bounded domains introduces new challenges. Notably, we preserve the full boundary vorticity equation (4.10), including the third-order normal derivative term $\partial_{x_2}^3 u_1$, within our Monte Carlo scheme (see equation (4.14)). This differs from previous approaches (e.g., [1]), which typically omit such high-order terms. Retaining these contributions enables our method to better capture subtle boundary-layer effects, particularly in regions of strong shear.

Despite the generality of our stochastic framework, several limitations remain. Convergence results are currently available only for the unbounded case [6, 9] and for simple wall-bounded geometries such as the upper half-plane [2]. For more complex domains, such as the corner or belt geometries, rigorous convergence or stability analysis remains open. Existing theoretical work (e.g., [12, 13]) has primarily focused on the formulation of stochastic representations, without deriving explicit error bounds or long-time stability results. On the computational side, the method remains costly

due to the large number of particles and the expensive evaluation of singular kernels arising from image or mirror techniques. Additionally, the framework is currently limited to domains with flat boundaries; its extension to curved or irregular geometries is a nontrivial direction for future investigation. Finally, the numerical evaluation of high-order derivatives near walls (such as the third-order normal derivative in the boundary vorticity equation) can introduce numerical sensitivity and potential instability.

Several promising directions remain for further development. To improve computational performance, fast summation techniques such as the Fast Multipole Method (FMM) could be incorporated, reducing the cost of Biot–Savart evaluations from $\mathcal{O}(N^2)$ to $\mathcal{O}(N \log N)$ or even $\mathcal{O}(N)$ [7]. While our current formulations apply to specific geometries with flat walls, more general domains may be handled using conformal mapping techniques, as suggested in [2]. However, convergence in such cases remains to be established. To improve the stability and accuracy of boundary derivative evaluations, future work might also incorporate automatic differentiation or higher-order finite difference schemes. Lastly, optimizing the algorithmic complexity is essential for extending the present Monte Carlo-based framework to three-dimensional flows, where the computational burden grows significantly with dimensionality.

Chapter 8

Conclusion

In this dissertation, we have developed a unified stochastic framework for simulating two-dimensional incompressible viscous flows using the random vortex method across a range of geometries. Building on classical formulations for unbounded domains, we extended the method to wall-bounded configurations and introduced novel methodologies for more intricate domains, including corner-shaped and belt-like geometries. In these complex settings, we constructed reflection-based Biot–Savart kernels and implemented boundary-layer corrections that preserve high-order derivative effects, enabling the accurate capture of subtle boundary-layer phenomena often neglected in prior approaches.

While our results demonstrate the flexibility and potential of the random vortex method, several challenges remain. Rigorous convergence analysis is currently available only for relatively simple geometries, and its extension to domains with multiple or nontrivial boundaries remains an open problem. Additionally, the high computational cost—especially for evaluating singular kernels and high-order derivatives near boundaries—limits the scalability of the method. Future work should focus on improving computational efficiency through fast summation techniques, adaptive meshing, or automatic differentiation, and on extending the framework to three-dimensional flows and more general geometries. These directions hold promise for advancing the applicability of stochastic vortex methods in computational fluid dynamics.

Bibliography

[1] V. Cherepanov, J.-G. Liu, and Z. Qian. On the dynamics of the boundary vorticity for incompressible viscous flows. *J. Sci. Comput.*, 99(42), 2024.

[2] V. Cherepanov, Z. Qian, and J. Wu. Monte-carlo simulations for wall-bounded fluid flows via random vortex method. *arXiv preprint arXiv:2208.13233*, 2022.

[3] A. J. Chorin. Numerical study of slightly viscous flow. *J. Fluid Mech.*, 57:785–796, 1973.

[4] G.-H. Cottet and P. D. Koumoutsakos. *Vortex Methods: Theory and Practice*. Cambridge University Press, Cambridge, 2000.

[5] L. C. Evans. *Partial Differential Equations*, volume 19 of *Graduate Studies in Mathematics*. American Mathematical Society, 2nd edition, 2010.

[6] J. Goodman. Convergence of the random vortex method. *Comm. Pure Appl. Math.*, 40(2):189–220, 1987.

[7] N. A. Gumerov and R. Duraiswami. Efficient fmm accelerated vortex methods in three dimensions via the lamb–helmholtz decomposition. *J. Comput. Phys.*, 245:302–322, 2013.

[8] J. Li, Z. Qian, and M. Xu. Twin brownian particle method for the study of oberbeck–boussinesq fluid flows. *arXiv preprint arXiv:2303.17260*, 2023.

[9] Y. Long. Convergence of the stochastic vortex method for the navier–stokes equations. *SIAM J. Numer. Anal.*, 25(1):1–17, 1988.

[10] A. Majda and A. Bertozzi. *Vorticity and Incompressible Flow*. Cambridge University Press, 2002.

[11] B. Øksendal. *Stochastic Differential Equations: An Introduction with Applications*. Springer, 6 edition, 2003.

[12] Z. Qian. Stochastic formulation of incompressible fluid flows in wall-bounded regions. *arXiv preprint arXiv:2206.05198*, 2022.

[13] Z. Qian, E. Süli, and Y. Zhang. Random vortex dynamics via functional stochastic differential equations. *Proc. R. Soc. A*, 478(2260):20220030, 2022.

[14] G. I. Taylor. Diffusion by continuous movements. *Proc. Lond. Math. Soc.*, s2-20(1):196–212, 1922.